Investigation of New Particle Formation mechanisms and aerosol processes

at the Marambio Station, Antarctic Peninsula.

Lauriane Lucie Josette Quéléver [1], Lubna Dada [1,2,3], Eija Asmi [4,5], Janne Lampilahti [1], Tommy Chan [1],
Jonathan Ferrara [4], Gustavo Copes [4], German Pérez-Fogwill [4],
Luis Barreira [5], Minna Aurela [5], Douglas Worsnop [1,6],
Tuija Jokinen [1,7], and Mikko Sipilä [1]

[1] Institute for Atmospheric and Earth System Research / INAR-Physics, P.O. Box 64, FI-00014 University of Helsinki, Finland.
[2] Extreme Environments Research Laboratory, École Polytechnique Fédérale de Lausanne (EPFL) Valais, Sion, 1951, Switzerland
[3] Laboratory of Atmospheric Chemistry, Paul Scherrer Institute, 5232 Villigen, Switzerland
[4] Servicio Meteorológico Nacional / SMN, Av. Dorrego, 4019, Buenos Aires, Argentina
[5] Finnish Meteorological Institute / FMI, Erik Palmenin aukio 1, FI-00560 Helsinki, Finland
[6] Aerodyne Research, Inc. Billerica, MA 01821, USA
[7] The Cyprus Institute, The Climate & Atmosphere Research Centre (CARE-C), P.O. Box 27456 Nicosia, Cyprus

Corresponding Author:
Lauriane L. J. Quéléver (lauriane.quelever@helsinki.fi), Mikko Sipilä (mikko.sipila@helsinki.fi)

Abstract

Understanding chemical processes leading to the formation of atmospheric aerosol particles is crucial to improve our capabilities in predicting the future climate. However, those mechanisms are still inadequately characterized, especially in polar regions. In this study, we report observations of neutral and charged aerosol precursor molecules and chemical clusters composition (qualitatively and quantitatively), as well as air ions and aerosol particle number concentrations and size distributions from the Marambio research station (64°15'S - 56°38'W), located North of the Antarctic Peninsula. We conducted measurements during the austral summer, between 15 January and 25 February 2018. The scope of this study is to characterize New Particle Formation (NPF) event parameters and connect our observations of gas phase compounds with the formation of secondary aerosols to resolve the nucleation mechanisms at the molecular scale. NPF occurred on 40 % of measurement days. All NPF events were observed during days with high solar radiation, mostly with above freezing temperatures and, with low relative humidity. The averaged formation rate for 3 nm particles (J_3) was 0.686 cm^{-3} s^{-1} and the average particle growth rate ($GR_{3.8-12\ nm}$) was 4.2 nm h^{-1}. Analysis of neutral aerosol precursor molecules showed measurable concentrations of iodic acid (IA), sulfuric acid (SA) and methane sulfonic acid (MSA) throughout the entire measurement period with significant increase of MSA and SA concentrations during NPF events. We highlight SA as a key contributor to NPF processes, while IA and MSA would likely only contribute to particle growth. Mechanistically, anion clusters containing ammonia/ dimethylamine (DMA) and SA were identified, suggesting significant concentration ammonia and DMA as well. Those species are likely contributing to NPF events since SA alone is not sufficient to explain observed nucleation rates.

Here, we provide evidence of the marine origin of the measured chemical precursors and discuss their potential contribution to the aerosol phase.

1 Introduction

Atmospheric aerosol particles impact the planetary energy budget and radiation balance by influencing cloud optical properties and cloud lifetime (IPCC, 2013). Even though they are crucial for regulating the climate, aerosol particles remain insufficiently characterized, especially in remote regions (Schmale et al., 2019). Understanding the atmospheric processes in places where anthropogenic influence is minimal, such as polar regions, is important for characterizing the pre-industrial-like atmosphere. At the same time, polar environments are significantly impacted by human-induced climate change and are warming twice as fast as the global average (Stuecker et al., 2018). Additionally, polar ecosystems and landscapes are more and more being disturbed by increasing average temperatures that further affect emissions of trace gases into the atmosphere.

Aerosol particles have been observed and characterized in many places in the Arctic and Antarctica (Shaw, 1979; Shaw, 1988; Asmi et al., 2010; Kerminen et al., 2018; Sipilä et al., 2016; Dall´Osto et al., 2017; Jokinen et al., 2018; Dall´Osto et al., 2018; Herenz et al., 2019; Baccarini et al., 2020; Dall'Osto et al., 2019; Beck et al., 2021; Brean et al., 2021). Antarctic primary particles, mainly originating from sea spray or blowing snow, only weakly contribute to total particle number concentration (Lachlan-Cope et al., 2020). Modelling studies have estimated that primary particles would only contribute to ~2 % of the total particle count that the ground level in Antarctica (Merikanto et al., 2009). Secondary formation of aerosol particles, on the other hand, is believed to be the principal contributor to cloud condensation nuclei (CCN), especially in the Antarctic peninsula were models showed contributions varying from 75% up to 100 % (Jokinen et al., 2018; Kerminen et al., 2018; Merikanto et al., 2009). These secondary aerosols originate from nucleation of gas phase molecules, typically condensing oxidation products of locally or regionally emitted vapors. Once formed, neutral or charged molecular clusters can grow by condensation of gases to sizes where they can act as CCN. The process of aerosol nucleation followed by subsequent growth is called new particle formation (NPF). Only a few studies have observed nucleation mode particles (sub-10 nm) from Antarctica - including oceanic, coastal, and continental areas - (Asmi et al., 2010; Virkkula et al., 2009; Järvinen et al., 2013; Kyrö et al., 2013; Weller et al., 2015; Jokinen et al., 2018; Kerminen et al., 2018; Lachlan-Cope et al., 2020; Brean et al., 2021) and only two of those report molecular clusters forming from precursor gases in coastal sites (Jokinen et al., 2018; Brean et al., 2021).

Previously identified aerosol precursor vapors include sulfuric acid (e.g., Kulmala et al., 2013; Sipilä et al., 2010), iodic acid (Sipilä et al., 2016; Baccarini et al., 2020) and iodous acid (He et al., 2021), or highly oxygenated organic molecules (e.g., HOMs, Ehn et al., 2014; Bianchi et al., 2019; Kirkby et al., 2016). On the other hand, nucleating ion clusters such as bisulfate ions with sulfuric acid and ammonia (e.g., Kirkby et al.,

2011; Yan et al., 2018; Jokinen et al., 2018; Beck et al., 2021), bisulfate ions and neutral sulfuric acid with dimethyl amine (DMA, Kürten et al., 2014), were previously identified to participate in aerosol formation processes.

At Marambio, Aboa, and Princess Elisabeth coastal Antarctic stations, air mass trajectories during NPF events indicated a dominant role of the Southern Ocean as a source of aerosol particles, which chemical aerosol composition analysis confirmed by the abundancy of e.g., marine-originated sulfates (Asmi et al., 2010; Herenz et al., 2019; Jokinen et al., 2018). These studies suggest that NPF is linked to sulfur-containing compounds originating from dimethyl sulfide ($(CH_3)_2S$, DMS). At the Antarctic coast, oceanic DMS concentrations are the highest during December to January (i.e., austral summer) with concentration that could exceed 15 nM within the upper 10 m layer of the ocean around the Peninsula compared to a yearly average of ~5 nM (Lana et al., 2011). DMS has two well-known oxidation products formed from gas-phase reaction with OH radicals: sulfuric acid (H_2SO_4, SA, formed via sulfur dioxide, SO_2) and methane sulfonic acid (CH_3SO_3H, MSA), which can then initiate particle formation and subsequent particle growth (Barnes et al., 2006; Mardyukov and Schreiner, 2018).

Iodic acid (IA) was also found to significantly contribute to NPF in marine and polar environments (Sipilä et al., 2016; Baccarini et al., 2020; He et al., 2021). Although the chemical production of iodic acid is not fully resolved, IA results from the oxidation of reactive iodine (He et al., 2021) – in the form of I_2, HIO, or intermediate I - itself sourcing from algae/phytoplankton emissions contained within the sea water/ice/snow and exchanged into the atmosphere (Saiz-Lopez and Von Glasow, 2012). At the Antarctic Peninsula, the Weddell Seaside – that undergoes consistent and recurrent phytoplankton bloom episodes every early spring - is a potential reservoir for iodic acid emissions, especially due to slower ice retreat during the austral summer and colder sea surface temperature than the Southern Ocean on the north and west-side of the peninsula (Atkinson et al., 2012; Von Berg et al., 2020).

This work aims at charactering the gas-phase aerosol precursors naturally emitted from the marine/ice ecosystem and from the Antarctic continent with comprehensive gas phase and aerosol measurements performed at the Marambio research station, Antarctica. We present our results characterizing atmospheric NPF events observed in the Antarctic Peninsula (in section 3.2). There, we provide an extensive analysis of number size distributions of atmospheric aerosols and naturally charged ions, from ~1 nm to 800 nm. We also report the formation rates (J) and growth rates (GR) of the observed particle formation events. Our core analysis (in section 3.3) describes gas-phase composition and NPF precursors by mass spectrometry measurements of the concentration of SA, MSA and IA (cf. section 3.3.1) and by identifying the composition of ambient ions present during NPF events (cf. section 3.3.2). Finally, in chapter 4, we combine our results for the chemical composition of both gas- and aerosol-phases to discuss sources of precursor vapors producing secondary aerosol in the Antarctic Peninsula.

2 Methods

2.1 Measurement site

In-situ atmospheric gas- and particle-phase measurements were performed at the Argentinian Antarctic Station Marambio (64°15'S - 56°38'W) located on the Seymour Island in the northeastern-most part of the Antarctic Peninsula. Geographically (cf. Fig. 1), the island is on the north edge of the Weddell Sea. The station is operated year-round, with extensive scientific and logistic activities during the austral summer. The campaign instrumentation was located inside a laboratory container, specifically designed for continuous atmospheric composition measurements, sufficiently away (approx. 800 m) from the station main buildings and ideally placed fore-wind from the airstrip to avoid interfering contamination signals in our measurements. Comprehensive measurements of atmospheric composition and meteorology have been carried out in this location since 2013. A description of the Marambio station surroundings, the measurement container, and some previous results can be found in earlier publications, e.g., Asmi et al. (2018).
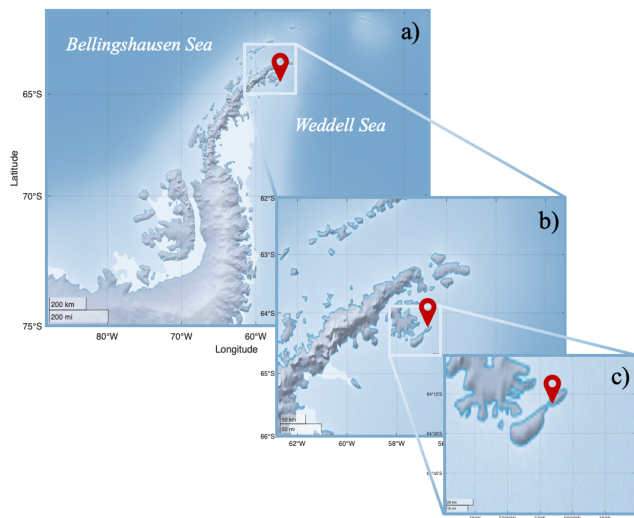
Figure 1: Map of the Antarctic Peninsula, a), with zoom in the north sector, b), and in the Seymour Island with the Marambio station, in c). The measurement location is indicated by the red pin.

2.2 Austral summer campaign 2018

The austral summer campaign in 2018 for measuring the precursors contributing to NPF at the Marambio station was planned for the warm season, when the probability of NPF occurrence is high (Fiebig et al., 2014; Kerminen et al., 2018). The aim was to characterize NPF events, formation, and growth parameters, and resolve the aerosol chemical precursors from their source to their chemical pathways leading to nucleation. We measured concentrations of size segregated aerosol particles (~ 1 – 800 nm diameter) from 19 January to 23 February and chemical information of possible gas-phase precursors from 30 January to 20 February, continuously (whenever possible).

2.3 Instrumentation

Measurements of aerosols and their gas-phase precursors

We deployed a large suite of instruments, briefly described below. Instrument principles and operations are given in detail in the *Supplementary Information*.

(1) The chemical composition and concentration of neutral molecules was measured by a nitrate-based Chemical Ionization Atmospheric Pressure interface Time Of Flight (CI-APi-TOF, Tofwerk A.G.) mass spectrometer (Jokinen et al., 2012). Its high-resolution analysis identifies and quantifies potential ambient gas-phase aerosol precursors, such as SA, MSA, IA, or HOMs. In some instances, we used the APi-TOF to directly measure atmospheric ions (i.e., naturally charged anions or cations), allowing only atmospheric ions to enter the instruments (i.e., with no added chemical ionization) (cf. *Supplementary information*).

(2) A nano Condensation Nucleus Counter (nCNC) combining a Particle Size Magnifier (PSM, Airmodus Ltd.) with a Condensation Particle Counter (CPC, Airmodus Ltd.) was employed to measure nano-particle concentration in the diameter range from 1 nm to 3 nm. The instrumentation and data inversions are extensively described in Vanhanen et al. (2011), Kangasluoma et al. (2016), Chan et al. (2020) and Lehtipalo et al. (2022) (cf. *Supplementary information*).

(3) A Neutral cluster and Air Ion Spectrometer (NAIS, Airel Ltd., Mirme and Mirme, 2013) provided number size distributions of neutral particles and naturally charged atmospheric clusters in the size range from 2 to 42 nm and from 0.8 to 42 nm, respectively. NAIS is well described in the literature and was operated according to the instructions of Manninen et al., 2016. (cf. *Supplementary information*).

(4) Aerosol particle size distributions were measured with a Differential Mobility Particle Sizer (DMPS): a Vienna-type Differential Mobility Analyzer (DMA) for particle size separation (Wiedensohler et al., 2012), followed by a Condensation Particle Counter (CPC; TSI model 3772) for particle counting. The particle size distribution was measured in 25 separate size bins at a 6-minute time resolution. This measurement has been

206 carried out continuously since the year 2013 but only data measured during the summer 2018 campaign are
207 presented here. (cf. *Supplementary information*).

208
209 The CI-APi-TOF, nCNC and NAIS were operated with individual (horizontal) inlet lines with a minimum
210 length (1 m, 0.8 m, and 0.9 m, respectively) to minimize losses of nanoparticles. The DMPS was operated in
211 the station's common inlet (PM10, Asmi et al., 2018) and equipped with an additional PM_1 cyclone to prevent
212 super micron particles from entering the setup.

213
214 ***Ancillary measurements***

215
216   Meteorological parameters were measured on the roof of the measurement container and recorded on
217 a data logger (QML201L, Vaisala Ltd.) since 2013. Measured parameters include temperature and relative
218 humidity (HMP155, Vaisala Ltd.), atmospheric pressure (PTB220, Vaisala Ltd.), wind speed and wind direc-
219 tion (ultrasonic anemometer: Thies 2D, Thies Clima), and radiation (pyranometer: CMP11, Kipp&Zonen).

220
221
222 ***Chemical composition of the aerosol phase***

223
224   Aerosol samples for chemical analysis were collected using a virtual impactor (VI, Loo and Cork,
225 1988), in which particles were divided to two size fractions (fine ($DP < 2.5$ μm) and coarse (2.5 μm < DP <
226 10 μm). Flow rate of the VI was 16.7 L.min^{-1}, of which 15 L.min^{-1} is used to collect the fine particles and the
227 remaining 1.7 L.min^{-1} is used for collection of the coarse particles. Particles were collected on 47-mm Teflon
228 filters. Sampling time was one week. Collected filters were stored on petri slides and kept in a freezer (−18
229 °C) until analysis.

230
231 The mass concentrations of sodium (Na+), ammonium ($NH4^+$), potassium (K+), magnesium ($Mg2^+$), calcium
232 ($Ca2^+$), chloride (Cl$^-$), nitrate (NO3$^-$), sulphate ($SO4^{2-}$), methane sulfonic acid (MSA) and oxalate were deter-
233 mined from the filter substrates. Cation and anion analyses were done simultaneously with two ion chroma-
234 tography systems (Dionex ICS-2000). Filters were extracted in 10 mL of Milli-Q water with 10-min gentle
235 rotation just before chemical analysis. The uncertainty of the IC analysis was estimated according to the anal-
236 ysis of standards as 5 % to 10 %, depending on the ion analyzed. In this study chemical composition of the
237 fine particles is only presented.

238
239   **2.4 Characteristics of New Particle Formation events**

240
241   NPF events were identified based on the appearance of particles in the nucleation mode (3 - 25 nm)
242 showing signs of growth (e.g., particles reaching > 10 nm). A classification method was originally proposed

245 by Dal Maso et al. (2005) based on DMPS data. In this study, we combined both DMPS and NAIS data to
246 extend our observations to smaller sizes (Dada et al., 2018).

247

248 Condensation sink (CS, s^{-1}), which is a measure of how rapid precursor vapor concentrations are lost to pre-
249 existing particles, was calculated using the particle number size distribution measured by the DMPS following
250 the method proposed by Kulmala et al. (2012).

251

252 Growth rates (GR) of particles between 3.8 nm to 12 nm were calculated using the 50 % appearance time
253 method (Lehtipalo et al., 2014; Dada et al., 2020). Formation rates ($J_{1.5}$, J_3, J_5, and J_{10}) were calculated using
254 the balance equation where the change in concentration of particles inside a size bin is equivalent to the
255 sources (J_{Dp}) minus the available sinks ($F_{Coag} + F_{Growth}$), as in Kulmala et al. (2012).

256

257   (1) $J_{Dp} = \frac{dN_{Dp}}{dt} + CoagS_{Dp} \cdot N_{Dp} + \frac{GR}{\Delta_{Dp}} \cdot N_{Dp}$

258 where Dp represents the lower diameter of the bin, N_{Dp} is the particle number concentration inside the size bin,
259 and GR is the growth rate of particles out of the bin. Δ_{Dp} is the difference between the upper and lower ends of
260 the size bin of interest.

261

262 The coagulation sink ($CoagS_{Dp}$) is a measure of how rapid freshly formed particles of diameter Dp are lost to
263 pre-existing particles by collision or coalescence and is calculated as follows:

264

265   (2) $CoagS_{Dp} = \int K(Dp, Dp') \, n\,(Dp') \, dDp' \cong \sum_{Dp=Dp}^{Dp'=maxK} K(Dp, Dp') \, N_{Dp'}$

266

267 where $K\,(Dp, Dp')$ is the coagulation coefficient of particle sizes Dp and Dp', those inside the bin of J_{Dp} and
268 those of pre-existing particles, respectively. $N_{Dp'}$ is the number concentration of the pre-existing particles.

269

270 In this work, the formation rates of 1.5 nm particles ($J_{1.5}$) were calculated using nCNC data in the size range of
271 1.5 nm to 3 nm. Formation rates J_3, J_5 and J_{10} were calculated using NAIS data (total particle mode – using the
272 DMA of negative voltage) at the size ranges of 3 - 7 nm, 5 - 9 nm, and 10 - 14 nm, respectively. During events
273 when the GR could not be calculated (i.e., four events in total) – due to the absence of continuous growth
274 within the size ranges -, a median growth rate calculated of all the events occurring in the same month was
275 used to estimate the formation rate as described by Kulmala et al. (2022).

276

277 In addition, the charged particle formation rates ($J^{\pm}_{1.5}$ and $J^{\pm}_2$) were calculated using ion number concentra-
278 tion measured by NAIS in both polarities, whenever possible, to determine the contribution of ion induced
279 nucleation to the overall formation rate, according to the following equation:

280

$$(3) \quad J_{Dp}^{\pm} = \frac{dN_{Dp}^{\pm}}{dt} + CoagS_{Dp} \cdot N_{Dp}^{\pm} + \frac{GR}{\Delta Dp} \cdot N_{Dp}^{\pm} + \alpha \cdot N_{Dp}^{\pm} \cdot N_{<Dp}^{\pm} - \chi \cdot N_{Dp} \cdot N_{<Dp}^{\pm}$$

where $N_{Dp}^{\pm}$ is the concentration of ion in a given size range with a lower limit of 1.5 or 2 nm (depending on the J associated size range) and the upper limit ΔDp being larger than that. The coefficient α is the ion-ion recombination coefficient and χ is the ion-aerosol attachment coefficient. α and χ were 1.6×10^{6} cm^{-3}cm^{-1} and 0.01×10^{6} cm^{-3}s^{-1}, respectively (Kulmala et al., 2012).

3 Results

3.1 Ambient conditions: Meteorological parameters

Ambient meteorological conditions during the campaign are presented in Figure 2. Many sunny days are observed, occurring with above-zero degrees Celsius ambient temperatures, high radiation, and relative humidity below 75 %. Even though the measurement site belongs to the Antarctic continent, its position - at relatively high latitude (64°15'S) - gives daily solar cycles with zero radiation during the short summer nighttime periods (cf. Fig. 2b). During daytime, higher radiation enhances photo-active emissions from the sea/land ecosystems and promotes atmospheric photochemistry. This is expected to lead to day-time appearance of gas-phase molecules and/or molecular clusters of condensing vapors that can lead to new particle formation and/or aerosol growth. Furthermore, since temperatures above freezing also lead to ice melting (especially in the Weddell Sea area), they are likely to enhance chemical fluxes between thinning ice, ocean, and air (Notz, 2009). These clear sky, warm, sunny days during summertime are known to be optimal weather conditions for NPF to occur in the mid-latitude regions (Dada et al., 2017) and in the Arctic (e.g., Beck et al. 2021) and Antarctic regions (Weller et al., 2015; Jokinen et al., 2018; Baccarini et al., 2020; Brean et al., 2021). Analysis of winds (cf. Fig. 2c) revealed that periods of the highest temperature are seen when wind is blowing from north, bringing warmer air across from the Southern Ocean. Predominant winds were seen from North-Northwest and South-Southwest sectors. The strongest winds were recorded from the South (180°), also driving primarily cold air from the continental plateau, agreeing with Asmi et al. (2018).

316
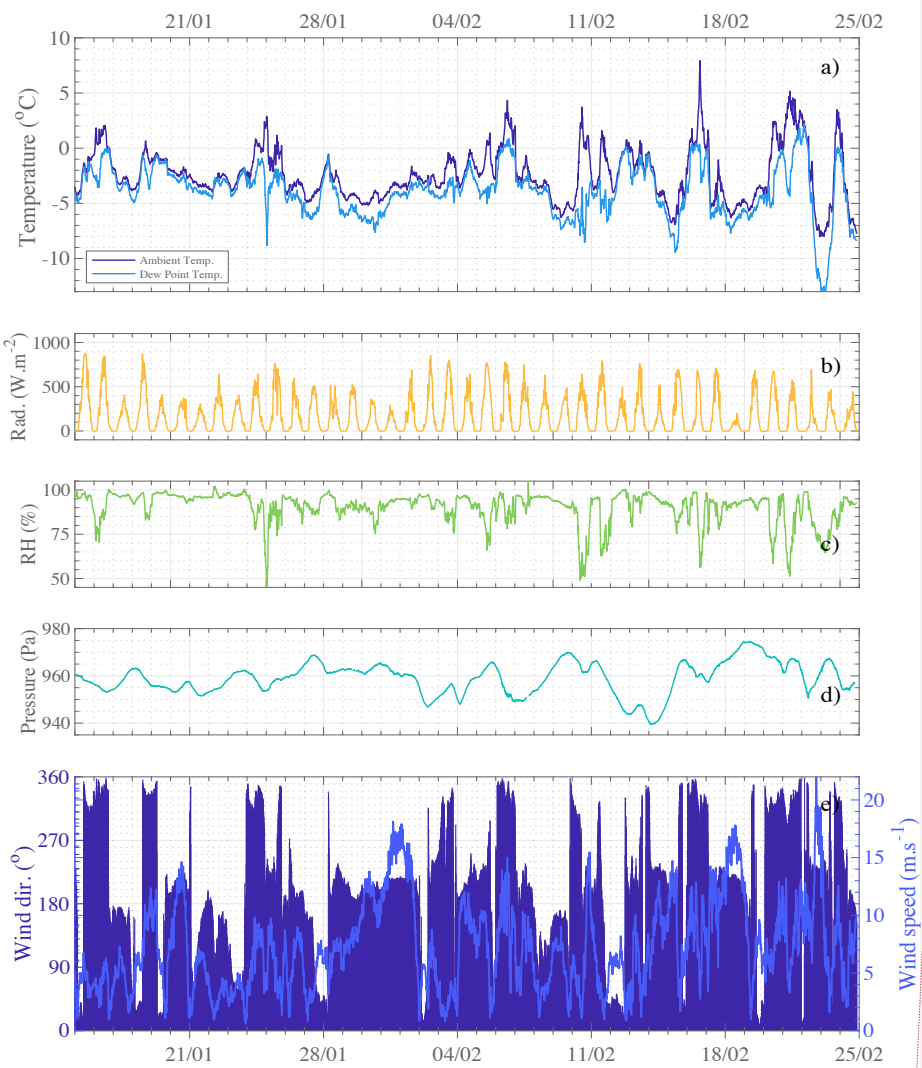
Figure 2: Time series of meteorological parameters: a) temperature (dark blue), dew point (light blue), b) global radiation (orange), c) relative humidity (light green), d) atmospheric pressure (blue green), e) wind direction (dark blue bars) and wind speed (medium blue line). The data are presented with a 10-min resolution and reference time set as local standard, UTC-3.

3.2 Observation & Characterization of NPF events

A total of 13 NPF events (occurring on 12 days) were observed during the 35-day summer campaign. Figure 3a shows the continuous size distribution series over the total measurement period from NAIS measurement (size range: 1.8 – 42 nm) and Figure 3b combined the data from nCNC (size shown: 1.2 – 2.7 nm), the NAIS (2.7 nm - 12 nm), and the DMPS (12 nm – 800 nm). Daily number size distribution plots are shown for the 12 event days separately in the *Supplementary Information* (Fig. S3) as well as continuous size distribution series for ion mode (Fig. S4).
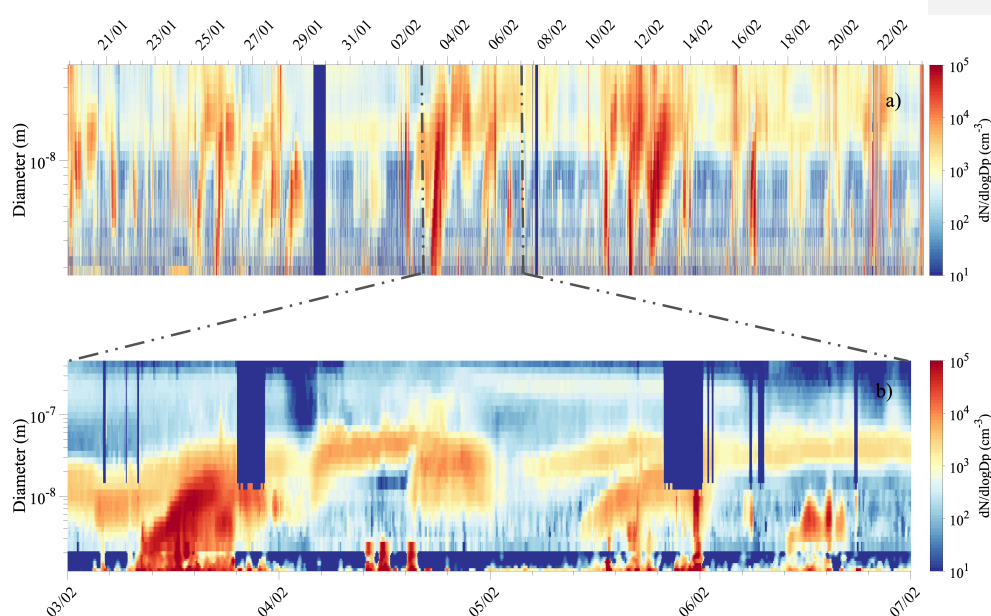
Figure 3: a) Number size distribution from NAIS measurement from 1.8 nm to 42 nm over the whole measurement campaign and **b)** combined size distribution of aerosol particle from 1.2 nm to 800 nm for 3-7 February 2018. The last surface plot combines data from nCNC (1.2 - 2.7 nm), NAIS (particle mode, 2.7 - 12 nm) and DMPS (12-800 nm), whenever the data were available and according to DMPS data flag (only unpolluted data are shown from the DMPS measurements).

During each of the NPF events observed during the campaign, high population of sub-3 nm aerosol particles were seen with concentration larger than 10^4 cm^{-3}. The particles were observed to grow to Aitken mode size range (25 - 100 nm) but rarely reached the accumulation mode sizes (i.e., > 100 nm) (cf. Fig. 3b). Strong NPF events were identified before midday - local time - (66 % of events), lasting longer than events occurring later in the afternoon. Afternoon events (33 % of the total events) never lasted longer than 2.5 hours. NPF events

354 did vary from day to day: On certain days, growth of the particles was interrupted by abrupt changes in wind

355 direction - resulting in an inability to retrieve a growth or a formation rate within reasonable uncertainty (e.g.,

356 28 January) -; on other days multiple NPF events were observed (e.g., 16 February); or NPF events appeared

357 to have a bumped shape – appearing sporadically - resembling those observed in the Arctic by Beck et al.

358 (2021) as the events observed on 28 January and 6 February.

359

360 Formation rates were calculated for particle sizes of 1.5, 2, 3, 5 and 10 nm particles, as summarized in Table

361 1. These formation rates were calculated for the smallest possible particles but also for bigger sizes to ease the

362 comparison with the literature.

363

364 Formation rates of 1.5 nm particles (i.e., $J_{1.5}$) were surprisingly high, reaching the maximum rates of 9.2, 10.0,

365 or even 19 cm^{-3} s^{-1}, on Feb. 11th, 10th, and 3rd, respectively. These significantly high values are comparable to

366 those calculated for highly vegetated rural location or even urban areas (e.g., Deng et al., 2020; Kontkanen et

367 al., 2016; Yu et al., 2014), which is surprising due to the remote nature of the environment at our measurement

368 site. For example, formation rates for 1.5 nm particle on the order of 0.030 - 0.013 cm^{-3} s^{-1} were estimated for

369 the Aboa research station on the other side of the Weddell Sea in East Antarctica (Jokinen et al. 2018). A recent

370 study observing nucleation phenomena at the peninsula close by our measurement location (Brean et al., 2021)

371 found a remarkably high $J_{1.7}$ value reaching up to 3.07 cm^{-3} s^{-1} but still lower than our observed values. Alt-

372 hough the formation rates at 1.5 nm are higher than those reported previously, the rates for larger particles

373 (i.e., J_3, J_5, J_{10}) are comparable with the previously reported studies. This discrepancy between formations rates

374 of 1.5 nm particles and of bigger particles could be attributed to favorable nucleation conditions (i.e., sufficient

375 nucleating vapors) but a lack of condensable vapors contributing to particle growth which, in all, reduces the

376 probability of particle survival.

377

378 The nucleation rates for 3 nm particles in our study ranged from 0.13 cm^{-3} s^{-1} to 3 cm^{-3} s^{-1} , which were, on

379 average, also significantly higher than 0.03 cm^{-3} s^{-1} < J_3 < 0.14 cm^{-3} s^{-1} reported from Jokinen et al. (2018)

380 study or from Kecorius et al. (2019) who showed J_3 values from 0.080 cm^{-3} s^{-1} to 0.319 cm^{-3} s^{-1} during a polar

381 cruise in the Arctic. On the other hand, our observation agrees with the J_{10} reported by Kyrö et al. (2013)

382 ranging from 0.003 to 0.3 cm^{-3} s^{-1}, with 0.006 cm^{-3} s^{-1} < J_{10} < 0.37 cm^{-3} s^{-1} in our case.

383

384 Additionally, to account for ion induced nucleation, we calculated the formation rates for charged ions of 1.5

385 nm ($J^{+/-}_{1.5}$) separately using the ion concentrations measured with the (N)AIS in ion mode. The formation rates

386 for positive 1.5 ions, $J^+_{1.5}$, ranged from 3.6 × 10^{-4} to 8.3 × 10^{-2} cm^{-3} s^{-1} and $J^-_{1.5}$ was from 2.2 × 10^{-3} to 5.4 × 10^{-2} cm^{-3} s^{-1}. Our results are significantly lower than the maximum $J_{1.5}$ of 0.33 cm^{-3} s^{-1} reported in Beck et al.

388 (2021) or from Kyrö et al. (2013) who showed 0.02 cm^{-3} s^{-1} < $J_{1.6}$ < 4.2 cm^{-3} s^{-1} - in two coastal Antarctic sites,

389 but in the range reported from the Arctic ocean by Kecorius et al. (2019, e.g., 0.026 cm^{-3} s^{-1} < $J_{1.6}$ < 0.060 cm^{-3}.s^{-1}). In comparison to 1.5 nm-neutral particle formation rates, the ion formation rates do not represent a major

400 contribution (ratio $J_{neutral}/J_{ion} \sim 10^3$), implying that the relatively high neutral nucleation rates are not primarily

401 due to ion-mediated nucleation.

402

403 Particle growth rates were calculated for 3.8 nm to 12 nm diameter size or alternatively up to 11 nm and 8 nm

404 for event #1 and event #13, respectively, whenever the shape of the number size distribution was continuously

405 increasing. Averages for each event are also presented in Table 1. Similarly to formation rates of the smallest

406 particles, the growth rates were remarkably higher (1.2 nm h^{-1} < GR < 10.9 nm h^{-1}) than previously reported

407 for other Antarctic sites. In comparison, Weller et al. (2015) reported growth rates from 3 to 25 nm particles

408 ranging from 0.06 to 0.9 nm h^{-1} at Neumayer III station, Jokinen et al. (2018) showed 0.26 nm h^{-1} < GR < 1.30

409 nm h^{-1} at Aboa and Brean et al. (2021) published growth rates for 4.5 - 10 nm particles of 0.41 nm h^{-1} to 0.58

410 nm h^{-1} measured at the Peninsula. Additionally, Kerminen et al. (2018) reviewed aerosol characterization from

411 many different field studies and indicated an upper growth rate estimation of 5.5 nm h^{-1} (as 95th percentile) in

412 Antarctic sites versus 4.1 nm h^{-1} in Arctic environments. Recent Arctic studies by Kecorius et al. (2019)

413 reported 0.62 nm h^{-1} < GR $_{(3-7\ nm)}$ < 4.25 nm h^{-1} while Collins et al. (2017) reported averaged growth rates of

414 4.3 ± 4.1 nm h^{-1}.

415

Commented [QLLJ26]: RC2>>TC9

Commented [QLLJ27]: RC1>>C2

417 **Table 1:** Summary of NPF event classification, formation and growth parameters calculated during the Marambio austral summer campaign. The pollution flag is determined based on DMP
418 according to NILU/EBAS format classification at the start time of the event (when data available, 000: clean data, 189: data coming from a possibly polluted sector (e.g., station main buil
419 599: suspected pollution from unknown source). All formation rates are averaged between the start and end of the characterized events.

#	Date (dd/mm)	Start Time (SLT*, hh.mm)	Duration (hh.mm)	Flag (DMPS)	Formation Rates (J_{size}, cm.s^{-1}) $J_{1.5}$ ($J_{1.5^-}/J_{1.5^+}$)	(J_{2^-}/J_{2^+})	J_3	J_5	J_{10}	Condensation Sink (s^{-1})	Growth Rates ($Gr_{3.8-12^{**}}$
1	19/01	14.35	0.55	189	-	-	-	-	-	-	9.7 ± 3.2 (G
2	24/01	18.30	2.26	-	- ($1.3e^{-2}$ / $1.2e^{-2}$)	($1.2e^{-2}$ / $1.9e^{-2}$)	$6.0e^{-1}$	$3.3e^{-2}$	$6.1e^{-3}$	-	$2.4 \pm 0.$
3	25/01	14.00	2.25	000	- ($1.2e^{-2}$ / $9.8e^{-3}$)	($4.9e^{-1}$ / $6.9e^{-1}$)	1.2	$4.7e^{-1}$	$3.7e^{-1}$	$7.5e^{-4}$	10.9 ± 2
4	27/01	18.50	2.06	189	4.3 ($3.6e^{-4}$ /$3.6e^{-3}$)	($6.5e^{-3}$/$2.0e^{-2}$)	$6.9e^{-1}$	$7.2e^{-1}$	$1.8e^{-1}$	$3.8e^{-4}$	-
5	28/01	9.13	7.25	000	3.6 ($8.5e^{-3}$ /$6.7e^{-3}$)	($1.9e^{-2}$/$3.4e^{-2}$)	$1.6e^{-1}$	$4.8e^{-2}$	$1.2e^{-2}$	$2.2e^{-4}$	-
6	03/02	8.13	7.04	~000	19.0 ($3.4e^{-2}$/ $2.5e^{-2}$)	(2.9/4.0)	3.0	$5.5e^{-1}$	$2.9e^{-1}$	$1.1e^{-3}$	$2.4 \pm 0.$
7	05/02	8.35	6.36	000	1.5 ($7.2e^{-3}$/$5.2e^{-3}$)	($3.9e^{-3}$/$4.3e^{-3}$)	$1.8e^{-1}$	$1.3e^{-1}$	$6.8e^{-2}$	$1.3e^{-3}$	$1.6 \pm 0.$
8	06/02	9.35	4.25	000	1.1 ($8.3e^{-2}$/$5.4e^{-2}$)	(2.7/1.7)	$1.3e^{-1}$	$9.0e^{-3}$	$1.2e^{-2}$	$4.8e^{-4}$	$2.4 \pm 1.$
9	10/02	11.16	3.52	~000	10.0 ($4.2e^{-3}$/$2.2e^{-3}$)	($1.8e^{-1}$/$2.1e^{-1}$)	$8.3e^{-1}$	$3.6e^{-1}$	$3.6e^{-2}$	$3.7e^{-4}$	-
10	11/02	10.27	6.16	000	9.2 (-/-)	(1.3/$8.9e^{-1}$)	$9.2e^{-1}$	$3.5e^{-1}$	$2.1e^{-1}$	$4.0e^{-4}$	-
11	12/02	10.40	5.40	189	- ($8.1e^{-3}$ /$1.9e^{-2}$)	($4.1e^{-1}$/$5.9e^{-1}$)	2.1	2.7	$1.8e^{-1}$	$2.2e^{-3}$	$1.2 \pm 0.$
12 13	16/02	11.18	6.03	599	3.7 ($5.9e^{-2}$/$3.2e^{-2}$) -	($7.2e^{-2}$/$4.3e^{-2}$) -	$5.9e^{-1}$ -	$4.0e^{-1}$ -	$1.2e^{-1}$ -	$2.4e^{-5}$ -	$3.6 \pm 0.$ 2.2 ± 2.9 (G

* Standard local time, UTC -3
** Growth rates were calculated ideally from 3.8 nm to 12 nm. If the growth on that range cannot be determined in that range, the specific range is indicated in subscript as Gr_{x-x}.

3.3 Chemical composition of the gas-phase precursor molecules

3.3.1 Gas-phase contribution to NPF

Measurements utilizing nitrate based chemical ionization mass spectrometry (CI-APi-TOF) detected gas-phase molecules and molecular clusters that have affinity for proton transfer with nitrate reagent ion. These included SA, MSA, and IA, detected as HSO_4^- and $HNO_3HSO_4^-$ (m/z 96.9601 Th and 159.9557 Th), $CH_3SO_3^-$ and $HNO_3CH_3SO_3^-$ (m/z 94.9808 Th and 157.9765 Th), IO_3^- and $HNO_3IO_3^-$ (m/z 174.8898 Th and 237.8854 Th), respectively. Concentrations were calculated from high resolution peak fitting and reported below. The time series of those compounds during the whole campaign, according to the data availability of the CI operation, are shown in Figure 4.

The measured gas-phase concentrations of the species of interest showed maxima of $\sim 2.6 \times 10^7$ molecules cm^{-3}, $\sim 2.3 \times 10^7$ molecules cm^{-3} and $\sim 3.6 \times 10^6$ molecules cm^{-3} for the total SA, MSA, and IA concentrations, respectively. The three gas-phase compounds seemed to evolve with roughly similar behavior, likely due to favorable weather conditions promoting atmospheric chemical reactions and especially by enhancing photochemical oxidation reactions within a stable boundary layer. A significant and simultaneous increase in SA, MSA, IA concentrations was observed during peaking radiation time close to noon-time – coinciding with local zenith time, i.e., solar noon that is slightly later than midday - and prior to many NPF events, though to a smaller extent for IA. This clearly demonstrates the diurnal nature of the emission of those species, and their transport – especially for SA and IA – as shown in Figure 5. Additionally, it is worth mentioning that even though the MSA concentrations were on average higher than those of SA, event days correlated strongly with peaking SA concentration (then becoming higher than MSA concentration) while IA – whose concentration remained unchanged independently of NPF occurrence - was significantly lower than SA or MSA concentrations.

451
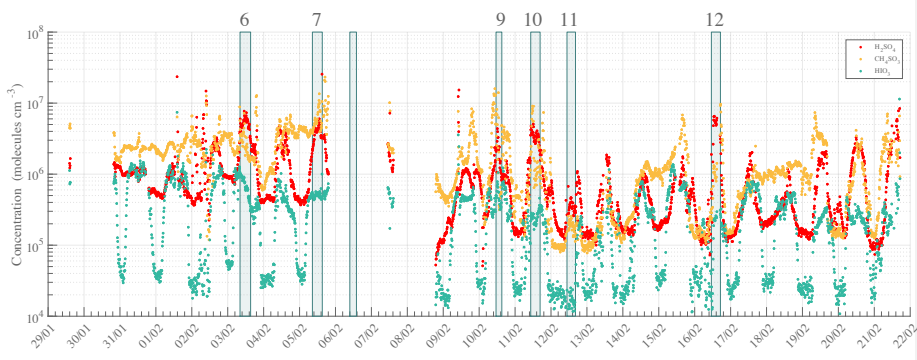
Figure 4: High resolution time series of H_2SO_4 (SA, red), CH_4SO_3 (MSA, orange), HIO_3 (IA, green). Numbers specified on the top of the figure refer to the event number as introduced in the NPF analysis (Cf. Table 1). The data are averaged to 10 min with local time (UTC -3). Note that the missing points are due to switch of the measurement mode and / or data availability.

455

456
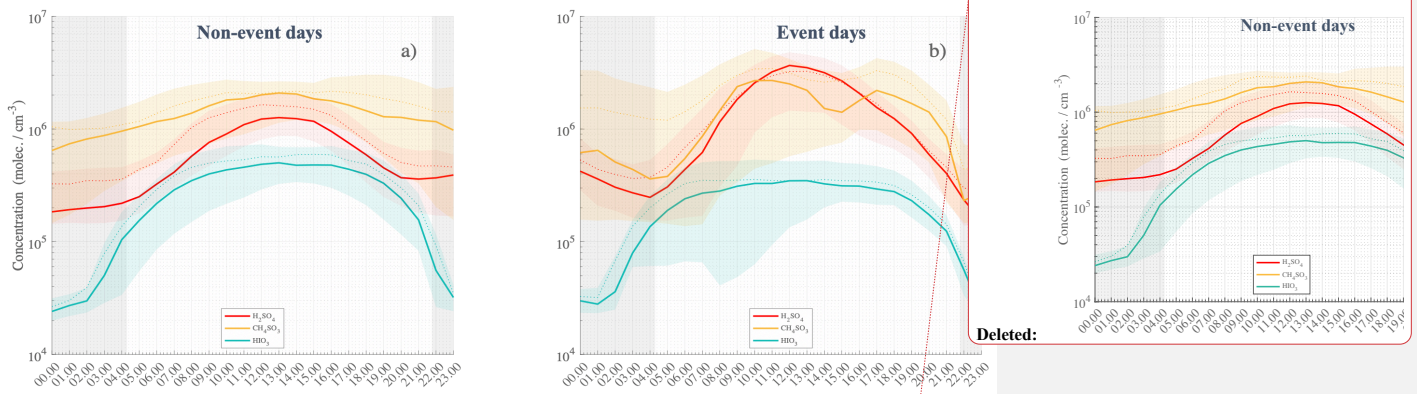
Figure 5: Statistical diurnal time series of H_2SO_4 (SA, red), CH_4SO_3 (MSA, orange), HIO_3 (IA, green) observed during non-event days a) and event days b). The solid lines represent the median hourly average concentrations, the dotted lines are the concentration means and the colored shaded areas show data points within the 25th and the 75th percentiles. Nighttime is represented by the gray-shaded area with median theoretical sunsets and sunrises occurring during the campaign. The actual sunset and sunrise values could vary approx. +/. 1.25 hours from the beginning to the end of the campaign.

462

Figure 5 shows the diurnal variations of SA, MSA and IA for event b) and non-event days a), separately. In both figures, we could see a clear rise in concentrations of SA, MSA and IA throughout the day, with maxima observed at midday. While both MSA and SA concentrations are on average increasing after sunrise, IA concentration started to increase already during nighttime, shortly after 01:00 SLT, suggesting that strong photo-chemistry conditions (i.e., direct solar radiation) might not be necessary to produce the observed IA agreeing

476 with He et al. (2021). Earlier studies have shown that IA is even anticorrelated with (still omnipresent) solar

477 radiation in more continental Antarctica (Jokinen et al., 2018). It is likely that even very low levels of solar

478 radiation would be sufficient to saturate the iodic acid production (Beck et al., 2021). Distinctively, a clear

479 difference in the statistical series can be seen between event and non-event days, with more than doubled SA

480 concentrations at zenith-time (factor of 2.25). MSA concentrations are only slightly higher in the morning and

481 afternoon – with an apparent drop occurring from 14:00 to 16:00 – although the starting concentrations at

482 sunrise and sunset are also smaller, depicting strong concentration variability as compared to non-event days.

483 On the other hand, IA is on average lower during event-days – e.g., from ~ 4.5×10^5 molecules cm^{-3} vs ~ $3 \times$

484 10^5 molecules cm^{-3}, with a factor of 1.5 smaller at zenith-time. This last observation indicates that IA is likely

485 not a key contributor to particle formation, while the duo SA-MSA could influence the aerosol phase as already

486 suggested by Beck et al. (2021), Hodshire et al. (2019) and Willis et al. (2016).

487

488

489 ### 3.3.2 Molecular characterization of aerosol / ion precursors: Study case on Feb 16th

490

491 The aerosol event observed on 16 February was particularly interesting due to the occurrence of two

492 consecutive NPF events within the same day. An overview of both aerosol concentrations / parameters and

493 reactive trace gases concentrations for 16 February is shown in Figure 6 with a) the particle number size dis-

494 tribution series from NAIS measurement, b) time series of total particle concentration within several size

495 modes (i.e., cluster, nucleation, Aitken and accumulation), c) estimated J rates for 1.5, 3, 5 and 10 nm particle

496 and d) time series for SA, MSA and IA.

505
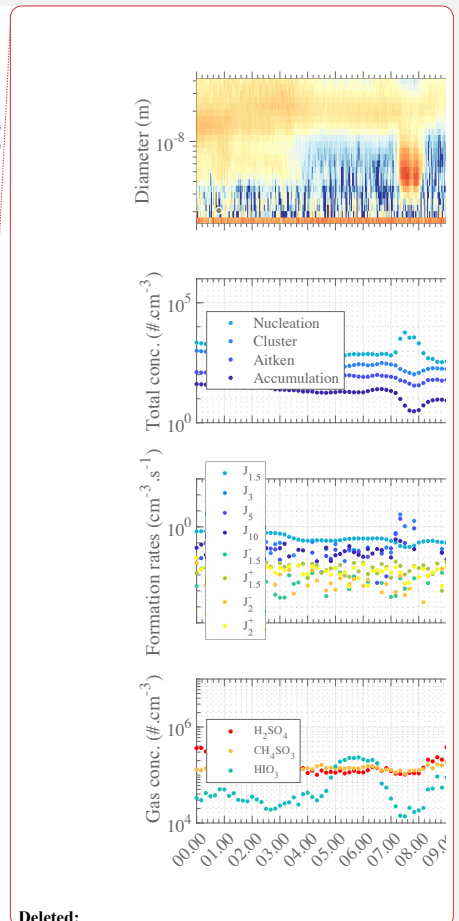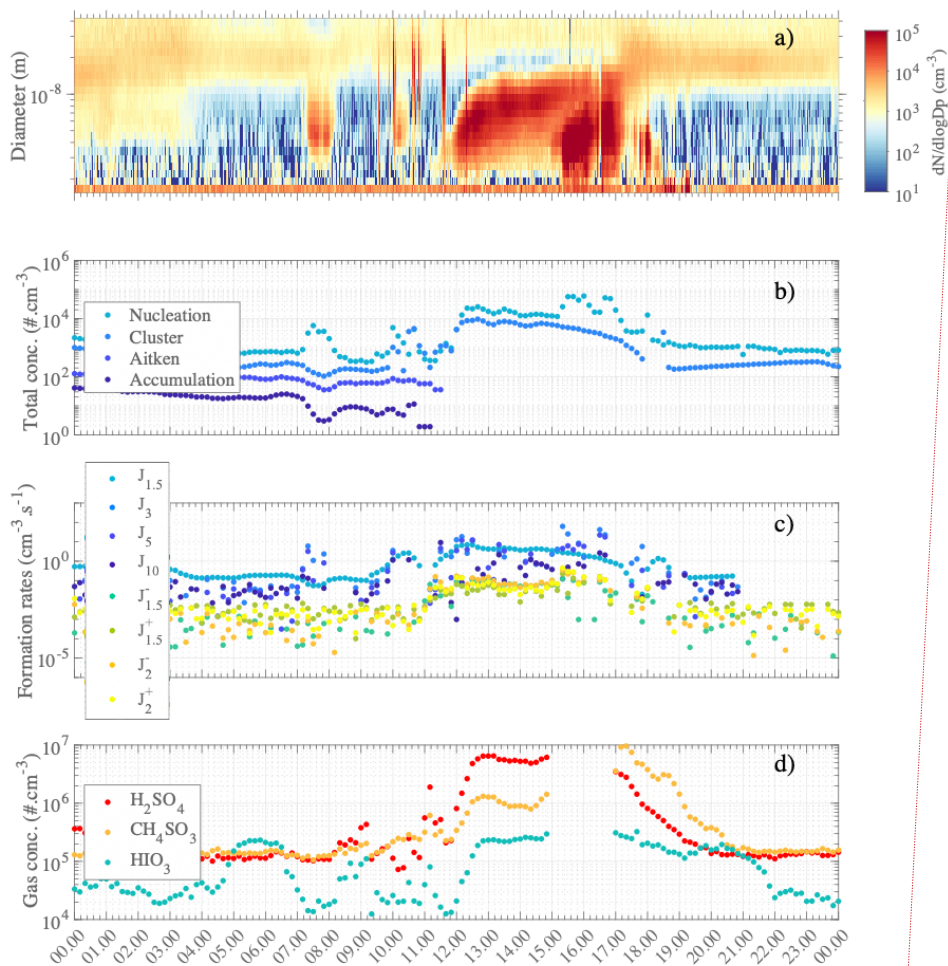
Figure 6: Overview of Aerosol formation event on February 16th, 2018: a) Number size distribution from NAIS measurements (Particle

506 mode). b) Concentrations of particles modes (cluster: sub- 3 nm – medium light blue, nucleation: 3 – 25 nm – light blue, Aitken: 25 –

507 100 nm – medium dark blue, accumulation: 100 – 1000 nm – dark blue). Note that the missing points for Aitken and Accumulation

508 mode are due to data filtering from suspected pollution from the DMPS data set. c) Formation rate estimation for $J_{1.5}$ (neutral – light

509 blue, (-) – blue green, (+) – green), J_2 ((-) - orange, (+) – yellow), J_3 (medium light blue), J_5 (medium dark blue) and J_{10} (dark blue).

510 Note that the formation rate calculation depends on the condensation/coagulation sinks calculated from the DMPS data. d) High reso-

511 lution time series of H_2SO_4 (red), CH_4SO_3 (orange), HIO_3 (green). Note that the data gap is due to ion mode of APi-measurement. All

512 data are averaged / estimated with a 10 min time resolution, with standard local time (UTC -3) as clock reference.

513

514 A clear NPF episode occurred from about 11:15 in the morning until sunset with a net increase of cluster and

515 nucleation mode particle concentrations. Close to noontime all trace gases of interest were significantly

523 increasing (Fig. 6d). MSA increased by almost a factor of 10 by 13:00 ($[MSA]_{t=13.00} = 1.3 \times 10^6$ molecules cm⁻

524 ³) and by more than 2 orders of magnitude at 16:00 ($[MSA]_{t=17.30} = 9.6 \times 10^6$ molecules cm⁻³) as compared by

525 the minimum baseline of $\sim 2 \times 10^5$ molecules cm⁻³ for both MSA and SA. SA maximum concentration was

526 6.5×10^6 molecules cm⁻³, also observed at 13:00.

527 IA concentrations were fluctuating throughout the day with maximum concentrations of $\sim 2.05 \times 10^5$ molecules

528 cm⁻³ and $\sim 2.35 \times 10^5$ molecules cm⁻³, respectively around 05:30 – 06:30 and shortly after 13:00. The net

529 increase of all these gas-phase species occurred quasi-simultaneously as the increase of formation rate of the

530 smallest particles and ions (Fig. 6c), occurring around noon. Interestingly, several sudden, short-lasting in-

531 creases for all SA, MSA, and IA concentrations were seen even before 13:00, matching bumps in nucleation

532 mode particles around 09:00 and 11:00 and one to two orders of magnitudes increase of cluster mode particles

533 at 11:00. The high concentrations of SA, MSA (and possibly IA) likely trigger the observed aerosol processes

534 (i.e., nucleation and/or growth of particles).

535

536 We investigated the mass spectrum further and show a complementary mass spectrum in Figure S2. Any highly

537 oxygenated organic molecules, HOMs (Bianchi et al., 2019; Ehn et al., 2014) could be reliably resolved from

538 the mass spectra analysis. We estimate that the total oxidized organic contribution, possibly condensable

539 HOM, did not exceed 5.5×10^6 molecules cm⁻³, between 16:30 and 17:30; assuming mass spectral peaks found

540 above 200 Th with positive mass defect could be HOMs (*cf. Supplementary*). However, the actual HOM con-

541 tribution is likely to be only a fraction of this estimation. Therefore, it is unlikely that HOM significantly

542 contributed to nucleation or growth of newly formed particles.

543

544 Specifically for this event, we complemented the CI-APi-TOF measurement with negative APi-TOF ambient

545 measurement mode, from 14:52 to 15:53, as reported in Table S1. By showing the divergence of the exact

546 molecular mass of a detected ion in high resolution from its integer mass (i.e., defined as mass defect), a mass

547 defect plot illustrates the mass defect of selected ions (in y-axis) over a studied mass range (in x-axis). Com-

548 pared to a typical mass spectrum this has the advantage to show the most significant ion population at once,

549 rather independently of signal intensity which is then scaled by the marker size, easing the identification of

550 e.g., clustering mechanisms as further discussed. There, each point of the mass defect plot corresponds to a

551 unique atomic composition. An example of such representation is shown in Figure 6, for the study case of 16

552 February.
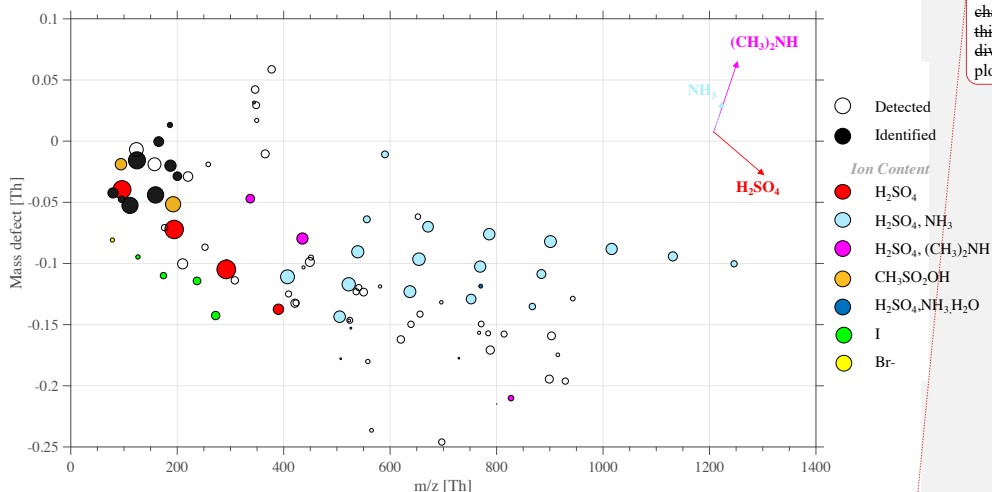
Figure 7: Mass defect plot for (-) APi-TOF measurements, on 16 February from 14.52 to 15.52. The figure type represents the deviation of high resolution fitted peaks exact mass normalized to the unit mass detected for each peak y-axis - e.g. $Br^-_{exact\ mass}$ = 78.9189, $Br^-_{unit\ mass}$ = 79, $Br^-_{mass\ defect}$ = - 0.0811 – while the x-axis represents the mass range (m/z). Data average is 1 hour for each spectrum to improve the signal to noise ratio and the peak shape statistics.

The APi-TOF ion mode showed TIC maximum values around 50 ions s[-1], detecting only ions that are naturally charged. The highest signals (i.e., intensity shown by marker sizes, cf. Fig. 7) are bisulfate and its multimers

$(H_2SO_4)_{0-4}HSO_4^-$, respectively at m/z = 96.9601, m/z = 194.9275, m/z = 292.8949 and m/z = 390.8622. Along with SA multimers, successive addition of sulfuric acid and ammonia NH_3 formed clusters represented with the light-blue dots, within the mass range 400 – 1250 Th. These sulfuric acid (bisulfate) - ammonia clusters were found with up to 10 additions of H_2SO_4 and 9 NH_3 on top of the HSO_4^- core ion. In line with previous field observations (e.g., Schobesberger et al., 2015; Bianchi et al., 2016; Jokinen et al., 2018; Yan et al., 2018; Beck et al., 2021; Sipilä et al., 2021) and laboratory studies (e.g., Kirkby et al., 2011; Schobesberger et al., 2015) showed that ammonia is detected only in clusters with 3 or more H_2SO_4 molecules around the HSO_4^- core.

The numerous clusters containing both sulfuric acid and ammonia, as well as the high intensity of the respective cluster signal (depicted by the marker size in Figure 6) suggest a high concentration of such ion group in the gas-phase which also could indicate an ion induced nucleation driven by the ternary system SA-ammonia(-water) - similar to observations made by Jokinen et al. (2018) in East Antarctica as well as measured in multiple other locations around the globe (e.g., Bianchi et al., 2016; Yan et al., 2018; Beck et al., 2021; Sipilä et al., 2021).

590 Additional clusters containing SA and dimethyl amine ((CH3)$_2$NH, DMA), principally as

591 (H$_2$SO$_4$)$_2$.(CH$_3$)$_2$NH.HSO$_4^-$ (m/z = 337.9527) and as (H$_2$SO$_4$)$_3$.(CH$_3$)$_2$NH.HSO$_4^-$ (m/z = 435.9210) but also one

592 larger cluster, (H$_2$SO$_4$)$_7$.(CH$_3$)$_2$NH.HSO$_4^-$ (m/z = 827.7893) was identified. Similarly to the finding of Brean et

593 al. (2021) who detected various SA-amine clusters around the peninsula, SA-DMA-H$_2$O driven nucleation

594 could also occur leading to formation rates significantly higher than those observed in the SA-NH$_3$-H$_2$O system

595 (Kürten et al., 2014; Almeida et al., 2013). In fact, as shown in laboratory studies, (negative) ion composition

596 from APi-TOF analysis likely matches the cluster composition of the neutral clusters in NPF (Schobesberger

597 et al., 2013). The appearance of DMA in the SA dimer and trimer suggests sufficient DMA to trigger nuclea-

598 tion; while the NH$_3$ in larger clusters is consistent with much higher NH$_3$ gas concentrations that then dominate

599 nano-particle growth. This highlights that DMA is 1000 times more effective than NH$_3$ for nucleation; so that

600 sub-ppt DMA and 100 – 1000 ppt levels (and above) of NH$_3$ could explain the ion cluster distribution observed

601 in Figure 7.

602

603 Individual MSA-related ions can be identified (cf. Fig. 7, orange dots) at m/z = 94.9808 and m/z = 192.9482,

604 respectively. Several studies have shown the possible role of MSA in aerosol processes, including nucleation

605 (Hodshire et al., 2019) - especially with involvement on SA-DMA clusters (Bork et al., 2014). However, in

606 our case, MSA was only found as CH$_3$SO$_3^-$ and as CH$_3$SO$_3$H.HSO$_4^-$. MSA was not observed in larger clusters

607 solely composed of SA, NH$_3$ and DMA and therefore likely does not contribute to the nucleation observed on

608 that day (at least not through to negative ion pathway).

609

610 Finally, we identified the presence of halogen compounds, (cf. Fig. 7, yellow and green dots), such as Br$^-$ (m/z

611 = 78.9189), I$^-$ (m/z = 126.9050), IO$_3^-$ (m/z = 174.8898), HIO$_3$NO$_3^-$ (m/z = 237.8854), HIO$_3$HSO$_4^-$ (m/z =

612 272.8571). The presence of halogenated species as natural ions could also indicate that these compounds con-

613 tribute to aerosol processes. However, these ions were only identified as small halogen clusters of low molec-

614 ular weight and with only low signal intensity. Considering previous observations in the arctic and coastal

615 environment (Sipilä et al, 2016) only shows iodine-related nucleation as successive addition of multiple iodic

616 acid and water group, it is unlikely that IA promotes nucleation either through neutral or ion-induced mecha-
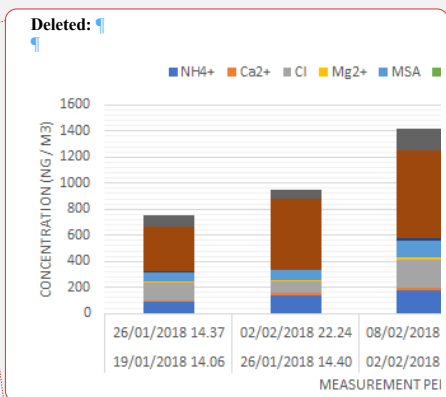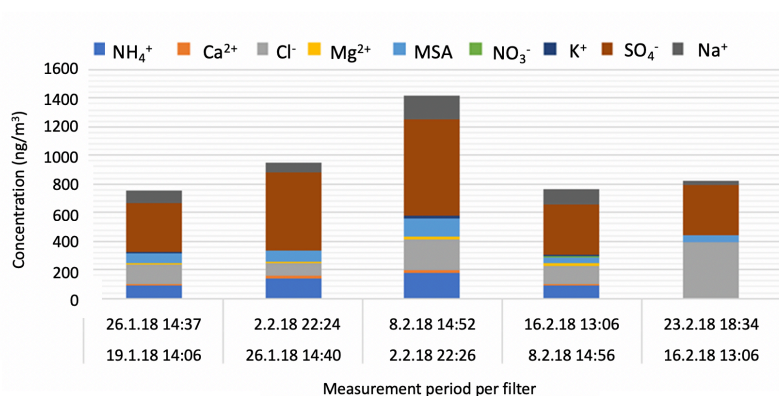
617 nism at this Antarctic site.

618

619

620

630 ### 3.3.3 Chemical composition of the aerosol phase

631

632 **Figure 8:** Chemical composition of water-soluble ions from weekly fine aerosol samples (PM2.5).

633   Asmi et al. (2018) reported aerosol chemical composition from weekly filter analysis containing ma-
634 rine–originated sea salt aerosols and the presence of ammonium, sulfate, nitrate and mesylate ($CH_3SO_3^-$). Here,
635 we performed the identical analysis, which agrees with the previously reported results.

636

637 Until February 16th, the fine aerosol composition remains rather constant with high amounts of non-sea salt
638 sulphate (nss-sulphate, i.e., sulphate - 0.246 × sodium - in mass concentration, Brewer (1975)) which is partly
639 neutralized by ammonia and a significant contribution from secondary marine MSA. The presence of Na^+, Cl^-
640 and Ca^{2+} ions also indicates contribution from primary marine sea salt and continental soil minerals. Aerosol
641 composition and mass concentrations are very similar to those found in Asmi et al. (2018) for Marambio
642 summer aerosol. The highest concentrations of ions are measured during the active nucleation period in the
643 beginning of February. By the end of the month, the concentrations of MSA, ammonium and calcium ions
644 decrease. No indications of anthropogenic contamination is found in the samples.

645

646 The bulk aerosol chemical composition (Fig. 8) reflects rather well the observed cycle of the secondary particle
647 formation and provides further evidence of the important role of sulphate/sulfuric acid, methane sulfonate, and
648 ammonia in the production and especially in the growth of Antarctic secondary aerosol. The qualitative agree-
649 ment of gas-phase and particle-phase compositions indicates that it is likely possible that these compounds
650 originate from similar marine/coastal sources.

651

652 ### 3.3.4 Source of gas-phase precursors

653

Backward trajectories from sampled air masses (Fig. 9) were analyzed and seen to originate mostly from the West sector passing through the Southern Ocean before surrounding the Peninsula from its Northwest side - coinciding with the observed wind directions. The observed trajectories could explain the low concentration of IA, whose variability was independent of NPF occurrence due to (1) the absence of travel over the Weddell littoral seaside prior to the NPF or (2) because the algae bloom on the melting sea ice – possibly responsible for an increase reactive iodine of organic origin- has already occurred earlier in the season. On the other hand, the air is clearly enriched in MSA and SA when passing over the ocean that has the highest DMS concentration over the Dec-Feb months (Lana et al., 2011). In some instances, air mass trajectories are seen to turn over the north of the peninsula, which can indicate a possible enrichment of gas produced by the fauna on the land or at the shore (e.g., local source of ammonia and amines from penguin colony established at approx. 8 km South of the sampling site during summertime). With a majority of trajectories originating from the Bellingshausen sea, NH_3 and various type of amines likelety originate from the (melting) ocean as discussed in Dall'Osto et al. (2017).

Figure 9c also shows altitudes of the air mass trajectories. While (Kerminen et al., 2018) reviewed that Antarctic NPF would easily take place within the free troposphere, both the number size distribution and the indicated altitude flight path point toward nucleation processes occurring at the surface layer considering the lifetime (λ) of key gas-phase precursors (e.g., $\lambda_{SA} < 0.5$ h, Fiedler et al. (2005)). Similar back trajectories were calculated for non-event days, separately for days with high SA concentrations (i.e., [SA] $> 2 \times 10^6$ molecules cm^{-3}) and for days with lower SA (Fig. S5a-c and Fig. 5a'-c', respectively). The result of the analysis as well as the model characteristics are shown in the *Supplementary Information*.

Commented [QLLJ45]: RC1>>C11

Commented [QLLJ46]: RC3 > C1,2,3

Commented [QLLJ47]: RC2>>TC19

Commented [QLLJ48]: RC2>>TC18
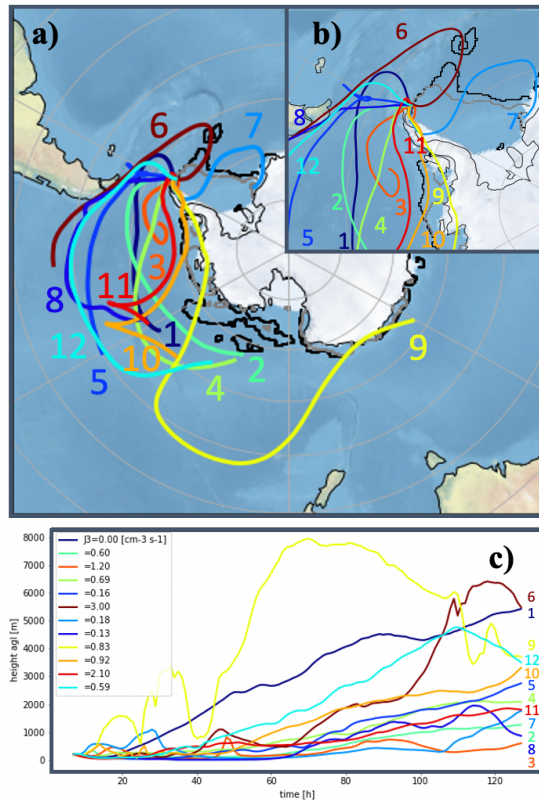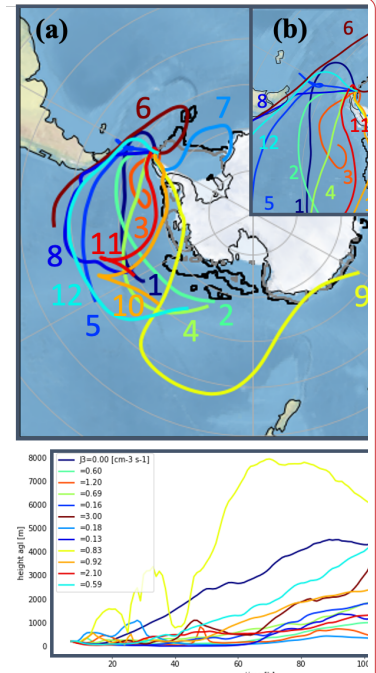
Figure 9: Backward trajectories for recorder NPF events a) (numbering according to classification Table 1). b) shows a zoom-in over the Antarctic Peninsula and c) shows the trajectory altitudes colored by formation rates J_3 values. In panel a) and b) the black and grey lines delimit the sea ice extent as average for January and February 2018, respectively. Sea ice data are from: ftp://sidads.colo-rado.edu/DATASETS/NOAA/G02135/south/monthly/ (Fetterer et al., 2017).

Local wind analysis (Fig. S6) was performed to determine possible local emission sources. In essence, no prevalent wind direction was found specifically for NPF days. However, in some instances, moderate to strong winds were seen to originate from the South/South-West sector where strong emission from the fauna is likely to occur by the shore at this season. Those days, 25 January (event # 3), 10 February (event # 9), and 11 Feb (event # 10), were among the highest growth ($GR_{3.8-12}$ = 10 nm h^{-1}) and the highest formation rates ($J_{1.5}$ = 10 cm^{-3} s^{-1} and $J_{1.5}$ = 9.2 cm^{-3} s^{-1}), respectively, which agree with our hypothesis attributing high emissions of e.g., ammonia / amines to the bird colony. On the other hand, Event #12 has a different trajectory and prevalent wind direction against the South sector. Given the fact that the anion mass defect (Fig.7) suggests significant presence of ammonia and possibly DMA on this event, specifically, nitrogen-containing base compounds origin can be explain by bio-mechanism from the zoo/phytoplankton in the Antarctic ocean.

4 Discussion

We observed the presence of many chemical constituents with significant measurable concentrations especially during aerosol formation events:

(1) IA daily maximum concentrations showed low variability, independent of NPF occurrence. Its concentration - only rarely over 10^6 molecules cm^{-3}- was unlikely sufficient to initiate NPF alone as compared with previously reported concentrations of 10^8 molecules cm^{-3} and (>) 8×10^6 molecules cm^{-3} for Arctic and coastal studies (Sipilä et al., 2016; Baccarini et al., 2020; Beck et al., 2021). Iodine emissions have been connected to sea-ice conditions and photolabile iodine compounds that are rapidly oxidized (Saiz-Lopez et al., 2015; He et al., 2021). The colder Weddell Sea provides high potential for the emission of iodine and thus iodic acid in the atmosphere. However, the temporality is a key factor governing such emissions. In fact, many studies have shown that IA concentration in polar-marine environment are usually peaking in early spring - already before the sea ice melt onset - (Saiz-Lopez et al., 2007) and during the refreezing transition period (Baccarini et al., 2020), strongly linking Iodic acid emissions with the sea ice state. This alternatively implies that our measurement period was then not optimum to catch iodine-related vapors maxima since the neighboring sea ice – key surface emission medium - was already melted around the Seymour Island. We do not exclude the possibility that IA would contribute to NPF in other seasons, but our data set show that during the summer period, from mid-January until the end of February, IA is likely not substantial.

The high concentrations of SA suggest that SA plays a key role in nucleation similarly to earlier observations from Antarctica (Jokinen et al., 2018) and from the Arctic (Beck et al., 2021). The significantly higher nucleation rates, with similar concentrations of SA, contrast with those studies that concluded that sulfuric acid – ammonia ion induced nucleation was the primary pathway to new particle formation. The reported new particle formation rates were systematically below 1 cm^{-3} s^{-1}, typically ca. 2 orders of magnitude lower than observed in our study despite comparable air temperatures.

Taking the case study of 16 February as an example, we found sulfuric acid – ammonia complexes with high abundancy from the analysis of natural ion chemical composition (Fig. 7). That would indicate that at least negative ion-induced nucleation pathways proceeds with sequential addition of SA and NH$_3$. However, the total nucleation rate was 3.6 cm^{-3} s^{-1} on this day, much larger than the negative ion induced nucleation rate of 0.06 cm^{-3} s^{-1}. This would lead to the conclusion that a neutral nucleation mechanism could dominate the process in our case.

Outside the case study, nucleation rates are still remarkably high, often exceeding the ion-induced nucleation rate limit set by ion-production rate of ca. 2 ion pairs cm^{-3} s^{-1} by galactic cosmic radiation. While the exact nature of neutral mechanism is not directly detected, the parameterization experiments performed in the CERN CLOUD-chamber (Dunne et al., 2016; Kürten, 2019) indicate that very high concentrations of ammonia would be needed to explain the observed nucleation rates – above ppb levels, under assumption that the ternary SA-NH$_3$-H$_2$O mechanism was solely responsible for initial nucleation.

(2) Another possibility is that dimethyl amine – as detected in negative ion spectra (cf. Fig. 7) - efficiently nucleates with sulfuric acid and could be primarily responsible for neutral new particle SA-H$_2$O-DMA formation pathway, as discussed in several studies (Kürten et al., 2014; Brean et al., 2021). Unfortunately, the deployed instrumentation does not allow the determination of DMA concentrations to assess the exact contribution of DMA on nucleation. Yet, our observation shows significantly higher nucleation rates than the reported values of both studies and, considering the range of measured SA concentrations, this conjecture is not likely to happen alone but rather as a possible synergetic effect of both amines and ammonia in the nucleation with sulfuric acid and water at the encountered temperatures.

(3) In addition to the high quantity of SA and MSA measured in CI mode, MSA was observed in ion cluster in form of CH$_3$SO$_3^-$ and MSA clusters with bisulfate ion but not in any larger nucleating cluster. Its contribution to a possible ion-induced nucleation mechanism is therefore unlikely in our case. However, we still cannot exclude the possibility that MSA would be weakly bounded to ion clusters and then evaporated inside the mass spectrometer vacuum chambers and lost in semi-energetic collisions within the electric fields used to focus ions inside the system. Additionally, mesylate (i.e., the MSA fragments - CH$_3$SO$_3^-$) were observed in significant fraction in the chemical speciation of the aerosol phase, which indicates its involvement in particle growth.

(4) The missing link is the (high) concentration of ammonia and amines required to follow the proposed SA-(NH$_3$/DMA)-H$_2$O nucleation scheme, likely on the order of ppb for ammonia and ppt levels for DMA. Without direct measurement of neither NH$_3$ nor DMA, we can only speculate that our observations point toward a strong source, possibly land-based (e.g., from high penguin population during summertime) or marine-based (e.g., emissions from planckton biological activity from the (melting) ocean). In fact, predominant wind possibly passing over a penguin colony at shore was seen from the wind roses proposed in Figure S6 for event 3, 4, 7, 9, and 10 and confirmed by the air mass trajectory analysis (Fig. 9). Yet, for our case study (event 12) - proving significant contribution of ammonia / DMA to detected in ion clusters -, nor the wind analysis nor the backward trajectory analysis point toward emission sourcing from the bird colony. We do not

Commented [QLLJ56]: RC2>>TC25
Deleted: CERN
Commented [QLLJ57]: RC2>>TC26
Deleted: sulfuric acid – ammonia – water
Formatted: Subscript
Formatted: Subscript
Deleted: 6

Formatted: List Paragraph, Line spacing: 1,5 lines, Numbered + Level: 1 + Numbering Style: 1, 2, 3, … + Start at: 1 + Alignment: Left + Aligned at: 1,27 cm + Indent at: 1,9 cm

Deleted: ¶
Formatted: Line spacing: 1,5 lines
Formatted: Font colour: Text 1
Deleted: ammonia
Formatted: Subscript
Formatted: Font colour: Text 1
Commented [QLLJ58]: RC1>>C11
Deleted: i
Formatted: Font colour: Text 1
Formatted: Font colour: Text 1
Deleted: 8
Formatted: Font colour: Text 1
Formatted: Font colour: Text 1
Formatted: Font colour: Text 1
Formatted: Font colour: Text 1
Formatted: Font colour: Text 1

exclude the possibility of additional influence from the local fauna, further away from the island, however, this nitrogen-containing species could also be marine-sourced, especially by emission from the metabolic activity of planktons and accumulation of precursors (e.g. proteins) in the melting sea ice (Dall'Osto et al., 2017). Ammonia and amine concentrations are key parameters that need to be assessed to fully understand the nucleation mechanism that our analysis suggests.

(5) MSA, together with DMA, NH$_3$ and SA, could potentially nucleate via a neutral, yet unidentified mechanism. However, this potential mechanism does not manifest itself in chemical composition of negative ion clusters, and potentially would only occur as neutral. It is also important to consider that our measurement relies on clusters that are stable enough to be analyzed in the very low-pressure chamber of the TOF, and thus might not be detectable with all species or molecular clus-ter possibly present in the real atmosphere. Further investigations of nucleation potential of MSA including the aforementioned compounds as mixture are required before MSA can be attributed to be responsible for our observed high nucleation rates that we observe at Marambio.

(6) To this remains the question of organics; our data set do not show substantial presence of HOMs (as characterized in forest environments), and possible detected compounds entering in our esti-mation – yet unidentified chemically, and which can also represent instrumental chemical back-ground – could be low-volatility organic compounds originating from marine environment that may contribute to the growth to some extent (Weller et al., 2015; Kecorius et al., 2019).

(7) A possible explanation for our observations of higher-than-expected nucleation and growth rates is that particle formation and growth could occur primarily at colder temperatures at higher alti-tudes, which would enhance both SA-NH$_3$ and SA-DMA nucleation. Nucleated particles would then be transported to lower altitudes resulting in apparently higher nucleation and growth rates. This in turn, suggest more regional emission sources rather than local emissions of SA, NH$_3$ or DMA as our analysis points toward. However, further investigations on vertical mixing would have been needed to confirm vertical distribution of nucleation and growth rates.

5 Conclusion

The Austral summer campaign 2018 at the Marambio Antarctic research station revealed very active aerosol processes and a frequency of new particle formation events of ~ 40 %. Out of 35 days of active meas-urement, a total of 13 NPF events were identified and characterized. In Marambio, NPF was promoted by key meteorological factors: high radiation (clear sky conditions), low humidity conditions (incl. the absence of precipitation), and high temperature – close to zero or above. We retrieved formation and growth rates for neutral and charged particles measured within 1.5 nm up to 800 nm size range - combining nCNC, NAIS and

840 DMPS instrumentation. As a reference, the formation rate of 3-nm (neutral) particles (J_3) during NPF was on
841 average 0.6863 cm^{-3} s^{-1} and the growth rate (GR $_{4\text{-}12\,nm}$) was on average 4.2 nm.h^{-1}. Those values are particularly
842 high in comparison with the literature, the comparison remains even more surprising considering the most
843 active NPF day where $J_{1.5}$ reached 19 $cm^{-3}s^{-1}$ and $GR_{4\text{-}12\,nm}$ was 10.9 nm.h^{-1}. The chemical analysis of gas-
844 phase aerosol precursors with CI-APi-TOF showed high concentrations of SA and MSA - on average 5.17 ×
845 10^5 molecules cm^{-3} and 1.18 × 10^6 molecules cm^{-3}, respectively – but quite low concentration of IA (on average
846 2.06 × 10^5 molecules cm^{-3}). All chemical species reached their maxima during mid-day (e.g., with maximum
847 concentration of 2.56 × 10^7, 2.32 × 10^7 molecules.cm^{-3}, respectively for SA and MSA during aerosol formation
848 events). The ubiquitously high SA concentration (peaking at almost 10^7 molecules cm^{-3} during many events)
849 and the high abundancy of SA-associated ion clusters makes no doubt on its involvement on NPF. The speci-
850 ation of negative ion spectra revealed clusters of dimethylamine – sulfuric acid – bisulfate-ions, as well as
851 various clusters of sulfuric acid - ammonia- bisulfate-ion - consistent with previously reported studies. How-
852 ever, the systematically high formation / growth rates cannot be quantitatively explained by SA-(DMA/ NH$_3$)-
853 H$_2$O NPF pathways without direct measurement of DMA and NH$_3$ gas phase concentrations. Additionally,
854 consistently high concentrations of MSA during daytime suggests a possible role of MSA in the growth, along
855 with SA and ammonia - as confirmed by the bulk aerosol chemical composition. Herein, the mechanism of
856 forming secondary aerosol in the peninsula involves a combination of SA, DMA, NH$_3$ and MSA (and only
857 relatively low contribution of IA, at least at this time of the year). Better understanding the synergetic effect
858 of DMA/NH$_3$ at these temperatures and environments require more field measurements and simulated exper-
859 iments, specifically including direct measurement of DMA and NH$_3$ concentrations.

860

861 **Data Availability**

862

863 *The data used in this work are available from the first author upon request. Please contact Lauriane L. J.*
864 *Quéléver (lauriane.quelever@helsinki.fi).*

865

866 **Acknowledgments**

867

868 This work was supported by the European Research Council under the following programs: ERC (GASPAR-
869 CON – grant n° 714621 & COALA – grant n° 638703) and EMME-CARE (grant n° 856612). We
870 acknowledge the support from the Academy of Finland (projects n° 296628 and n° 328290), the Center of
871 Excellence program (project n° 307331, 334514, 3282290), and Finnish Academy ACFA (project n° 335845
872 and ACCC Flagship funding (337552). We thank the generous help from the Servicio Meteorológico Nacional
873 - SMN, the Fuerza Aerea Argentina - FAA, and the FINNish Antarctic Research Program – FINNARP. We
874 are thankful for the technical personnel of the Marambio base for their support in cooperation, logistics and
875 measurements. We thank Toftools for providing mass spectrometry analysis tool package for MATLAB.

876

Author's Contribution

EA and **MS** supervised the project. **EA** initiated the measurement container deployment and is responsible for the large size aerosol and auxiliary measurements data from the measurement container. **LLJQ** co-organized the project, prepared, set up and performed the measurements, analyzed the data, and wrote the manuscript. **LLJQ** operated the instrumentation with the help of **EA, JEF** and **GEC. EA, MS** and **TJ** supervised the analysis and contributed to the scientific discussion in collaboration with **DW. LLJQ** analyzed the gas-phase measurements and produced most figures. **LD** processed, analyzed, and discussed the aerosol phase data, prepared by **TC, JL, GPF** and **EA**. **LB** and **MA** analyzed the chemical composition of bulk aerosols. **EA** performed the backward trajectory analysis and its relevant figures. All co-authors contributed to the scientific discussion, commenting and the revision of the manuscript.

Competing interests

The authors claim no competing interests.

Supplementary Information (*cf. Separate file***)**

References

Almeida, J., Schobesberger, S., Kürten, A., Ortega, I. K., Kupiainen-Määttä, O., Praplan, A. P., Adamov, A., Amorim, A., Bianchi, F., Breitenlechner, M., David, A., Dommen, J., Donahue, N. M., Downard, A., Dunne, E., Duplissy, J., Ehrhart, S., Flagan, R. C., Franchin, A., Guida, R., Hakala, J., Hansel, A., Heinritzi, M., Henschel, H., Jokinen, T., Junninen, H., Kajos, M., Kangasluoma, J., Keskinen, H., Kupc, A., Kurtén, T., Kvashin, A. N., Laaksonen, A., Lehtipalo, K., Leiminger, M., Leppä, J., Loukonen, V., Makhmutov, V., Mathot, S., McGrath, M. J., Nieminen, T., Olenius, T., Onnela, A., Petäjä, T., Riccobono, F., Riipinen, I., Rissanen, M., Rondo, L., Ruuskanen, T., Santos, F. D., Sarnela, N., Schallhart, S., Schnitzhofer, R., Seinfeld, J. H., Simon, M., Sipilä, M., Stozhkov, Y., Stratmann, F., Tomé, A., Tröstl, J., Tsagkogeorgas, G., Vaattovaara, P., Viisanen, Y., Virtanen, A., Vrtala, A., Wagner, P. E., Weingartner, E., Wex, H., Williamson, C., Wimmer, D., Ye, P., Yli-Juuti, T., Carslaw, K. S., Kulmala, M., Curtius, J., Baltensperger, U., Worsnop, D. R., Vehkamäki, H., and Kirkby, J.: Molecular understanding of sulphuric acid–amine particle nucleation in the atmosphere, Nature, 502, 359-363, 10.1038/nature12663, 2013.

Atkinson, H. M., Huang, R. J., Chance, R., Roscoe, H. K., Hughes, C., Davison, B., Schönhardt, A., Mahajan, A. S., Saiz-Lopez, A., Hoffmann, T., and Liss, P. S.: Iodine emissions from the sea ice of the Weddell Sea, Atmos. Chem. Phys., 12, 11229-11244, 10.5194/acp-12-11229-2012, 2012.

Asmi, E., Frey, A., Virkkula, A., Ehn, M., Manninen, H. E., Timonen, H., Tolonen-Kivimäki, O., Aurela, M., Hillamo, R., and Kulmala, M.: Hygroscopicity and chemical composition of Antarctic sub-micrometre aerosol particles and observations of new particle formation, Atmos. Chem. Phys., 10, 4253-4271, 10.5194/acp-10-4253-2010, 2010.

Asmi, E., Neitola, K., Teinilä, K., Rodriguez, E., Virkkula, A., Backman, J., Bloss, M., Jokela, J., Lihavainen, H., de Leeuw, G., Paatero, J., Aaltonen, V., Mei, M., Gambarte, G., Copes, G., Albertini, M., Fogwill, G. P., Ferrara, J., Barlasina, M. E., and Sánchez, R.: Primary sources control the variability of aerosol optical properties in the Antarctic Peninsula, Tellus B: Chemical and Physical Meteorology, 70, 1-16, 10.1080/16000889.2017.1414571, 2018.

Baccarini, A., Karlsson, L., Dommen, J., Duplessis, P., Vüllers, J., Brooks, I. M., Saiz-Lopez, A., Salter, M., Tjernström, M., Baltensperger, U., Zieger, P., and Schmale, J.: Frequent new particle formation over the high Arctic pack ice by enhanced iodine emissions, Nature Communications, 11, 4924, 10.1038/s41467-020-18551-0, 2020.

Barnes, I., Hjorth, J., and Mihalopoulos, N.: Dimethyl Sulfide and Dimethyl Sulfoxide and Their Oxidation in the Atmosphere, Chemical Reviews, 106, 940-975, 10.1021/acs.accounts.cr020529+, 2006.

Beck, L. J., Sarnela, N., Junninen, H., Hoppe, C. J. M., Garmash, O., Bianchi, F., Riva, M., Rose, C., Peräkylä, O., Wimmer, D., Kausiala, O., Jokinen, T., Ahonen, L., Mikkilä, J., Hakala, J., He, X.-C., Kontkanen, J., Wolf, K. K. E., Cappelletti, D., Mazzola, M., Traversi, R., Petroselli, C., Viola, A. P., Vitale, V., Lange, R., Massling, A., Nøjgaard, J. K., Krejci, R., Karlsson, L., Zieger, P., Jang, S., Lee, K., Vakkari, V., Lampilahti, J., Thakur, R. C., Leino, K., Kangasluoma, J., Duplissy, E.-M., Siivola, E., Marbouti, M., Tham, Y. J., Saiz-Lopez, A., Petäjä, T., Ehn, M., Worsnop, D. R., Skov, H., Kulmala, M., Kerminen, V.-M., and Sipilä, M.: Differing Mechanisms of New Particle Formation at Two Arctic Sites, Geophysical Research Letters, 48, e2020GL091334, 10.1029/2020GL091334, 2021.

Bianchi, F., Kurtén, T., Riva, M., Mohr, C., Rissanen, M. P., Roldin, P., Berndt, T., Crounse, J. D., Wennberg, P. O., Mentel, T. F., Wildt, J., Junninen, H., Jokinen, T., Kulmala, M., Worsnop, D. R., Thornton, J. A., Donahue, N., Kjaergaard, H. G., and Ehn, M.: Highly Oxygenated Organic Molecules (HOM) from Gas-Phase Autoxidation Involving Peroxy Radicals: A Key Contributor to Atmospheric Aerosol, Chemical Reviews, 119, 3472-3509, 10.1021/acs.chemrev.8b00395, 2019.

Bianchi, F., Tröstl, J., Junninen, H., Frege, C., Henne, S., Hoyle, C. R., Molteni, U., Herrmann, E., Adamov, A., Bukowiecki, N., Chen, X., Duplissy, J., Gysel, M., Hutterli, M., Kangasluoma, J., Kontkanen, J., Kürten, A., Manninen, H. E., Münch, S., Peräkylä, O., Petäjä, T., Rondo, L., Williamson, C., Weingartner, E., Curtius, J., Worsnop, D. R., Kulmala, M., Dommen, J., and Baltensperger, U.: New particle formation in the free troposphere: A question of chemistry and timing, Science, 352, 1109-1112, 10.1126/science.aad5456, 2016.

Bork, N., Elm, J., Olenius, T., and Vehkamäki, H.: Methane sulfonic acid-enhanced formation of molecular clusters of sulfuric acid and dimethyl amine, Atmos. Chem. Phys., 14, 12023-12030, 10.5194/acp-14-12023-2014, 2014.

Brean, J., Dall'Osto, M., Simó, R., Shi, Z., Beddows, D. C. S., and Harrison, R. M.: Open ocean and coastal new particle formation from sulfuric acid and amines around the Antarctic Peninsula, Nature Geoscience, 14, 383-388, 10.1038/s41561-021-00751-y, 2021.

Brewer, G. P.: Minor elements in seawater, Chemical Oceanography, 1, 415-496, 1975.

Chan, T., Cai, R., Ahonen, L. R., Liu, Y., Zhou, Y., Vanhanen, J., Dada, L., Chao, Y., Liu, Y., Wang, L., Kulmala, M., and Kangasluoma, J.: Assessment of particle size magnifier inversion methods to obtain the particle size distribution from atmospheric measurements, Atmos. Meas. Tech., 13, 4885-4898, 10.5194/amt-13-4885-2020, 2020.

Collins, D. B., Burkart, J., Chang, R. Y. W., Lizotte, M., Boivin-Rioux, A., Blais, M., Mungall, E. L., Boyer, M., Irish, V. E., Massé, G., Kunkel, D., Tremblay, J. É., Papakyriakou, T., Bertram, A. K., Bozem, H., Gosselin, M., Levasseur, M., and Abbatt, J. P. D.: Frequent ultrafine particle formation and growth in Canadian Arctic marine and coastal environments, Atmos. Chem. Phys., 17, 13119-13138, 10.5194/acp-17-13119-2017, 2017.

Dada, L., Chellapermal, R., Buenrostro Mazon, S., Paasonen, P., Lampilahti, J., Manninen, H. E., Junninen, H., Petäjä, T., Kerminen, V. M., and Kulmala, M.: Refined classification and characterization of atmospheric new-particle formation events using air ions, Atmos. Chem. Phys., 18, 17883-17893, 10.5194/acp-18-17883-2018, 2018.

968   Dada, L., Paasonen, P., Nieminen, T., Buenrostro Mazon, S., Kontkanen, J., Peräkylä, O., Lehtipalo, K.,
969   Hussein, T., Petäjä, T., Kerminen, V. M., Bäck, J., and Kulmala, M.: Long-term analysis of clear-sky new
970   particle formation events and nonevents in Hyytiälä, Atmos. Chem. Phys., 17, 6227-6241, 10.5194/acp-17-
971   6227-2017, 2017.

972   Dada, L., Lehtipalo, K., Kontkanen, J., Nieminen, T., Baalbaki, R., Ahonen, L., Duplissy, J., Yan, C., Chu, B.,
973   Petäjä, T., Lehtinen, K., Kerminen, V.-M., Kulmala, M., and Kangasluoma, J.: Formation and growth of sub-
974   3-nm aerosol particles in experimental chambers, Nature Protocols, 15, 1013-1040, 10.1038/s41596-019-
975   0274-z, 2020.

976   Dal Maso, M., Kulmala, M., Riipinen, I., Wagner, R., Hussein, T., Aalto, P. P., and Lehtinen, K. E.: Formation
977   and growth of fresh atmospheric aerosols: eight years of aerosol size distribution data from SMEAR II,
978   Hyytiala, Finland, Boreal Environment Research, 10, 323, 2005.

979   Dall'Osto, M., Beddows, D. C. S., Tunved, P., Harrison, R. M., Lupi, A., Vitale, V., Becagli, S., Traversi, R.,
980   Park, K. T., Yoon, Y. J., Massling, A., Skov, H., Lange, R., Strom, J., and Krejci, R.: Simultaneous
981   measurements of aerosol size distributions at three sites in the European high Arctic, Atmos. Chem. Phys., 19,
982   7377-7395, 10.5194/acp-19-7377-2019, 2019.

983   Dall´Osto, M., Geels, C., Beddows, D. C. S., Boertmann, D., Lange, R., Nøjgaard, J. K., Harrison, R. M.,
984   Simo, R., Skov, H., and Massling, A.: Regions of open water and melting sea ice drive new particle formation
985   in North East Greenland, Scientific Reports, 8, 6109, 10.1038/s41598-018-24426-8, 2018.

986   Dall´Osto, M., Beddows, D. C. S., Tunved, P., Krejci, R., Ström, J., Hansson, H. C., Yoon, Y. J., Park, K.-T.,
987   Becagli, S., Udisti, R., Onasch, T., O´Dowd, C. D., Simó, R., and Harrison, R. M.: Arctic sea ice melt leads to
988   atmospheric new particle formation, Scientific Reports, 7, 3318, 10.1038/s41598-017-03328-1, 2017.

989   Deng, C., Fu, Y., Dada, L., Yan, C., Cai, R., Yang, D., Zhou, Y., Yin, R., Lu, Y., Li, X., Qiao, X., Fan, X.,
990   Nie, W., Kontkanen, J., Kangasluoma, J., Chu, B., Ding, A., Kerminen, V.-M., Paasonen, P., Worsnop, D. R.,
991   Bianchi, F., Liu, Y., Zheng, J., Wang, L., Kulmala, M., and Jiang, J.: Seasonal Characteristics of New Particle
992   Formation and Growth in Urban Beijing, Environmental Science & Technology, 54, 8547-8557,
993   10.1021/acs.est.0c00808, 2020.

994   Dunne, E. M., Gordon, H., Kürten, A., Almeida, J., Duplissy, J., Williamson, C., Ortega, I. K., Pringle, K. J.,
995   Adamov, A., Baltensperger, U., Barmet, P., Benduhn, F., Bianchi, F., Breitenlechner, M., Clarke, A., Curtius,
996   J., Dommen, J., Donahue, N. M., Ehrhart, S., Flagan, R. C., Franchin, A., Guida, R., Hakala, J., Hansel, A.,
997   Heinritzi, M., Jokinen, T., Kangasluoma, J., Kirkby, J., Kulmala, M., Kupc, A., Lawler, M. J., Lehtipalo, K.,
998   Makhmutov, V., Mann, G., Mathot, S., Merikanto, J., Miettinen, P., Nenes, A., Onnela, A., Rap, A.,
999   Reddington, C. L., Riccobono, F., Richards, N. A., Rissanen, M. P., Rondo, L., Sarnela, N., Schobesberger,
1000 S., Sengupta, K., Simon, M., Sipilä, M., Smith, J. N., Stozkhov, Y., Tomé, A., Tröstl, J., Wagner, P. E.,
1001 Wimmer, D., Winkler, P. M., Worsnop, D. R., and Carslaw, K. S.: Global atmospheric particle formation from
1002 CERN CLOUD measurements, Science, 354, 1119-1124, 10.1126/science.aaf2649, 2016.

1003 Ehn, M., Thornton, J. A., Kleist, E., Sipilä, M., Junninen, H., Pullinen, I., Springer, M., Rubach, F., Tillmann,
1004 R., Lee, B., Lopez-Hilfiker, F., Andres, S., Acir, I.-H., Rissanen, M., Jokinen, T., Schobesberger, S.,
1005 Kangasluoma, J., Kontkanen, J., Nieminen, T., Kurtén, T., Nielsen, L. B., Jørgensen, S., Kjaergaard, H. G.,
1006 Canagaratna, M., Maso, M. D., Berndt, T., Petäjä, T., Wahner, A., Kerminen, V.-M., Kulmala, M., Worsnop,
1007 D. R., Wildt, J., and Mentel, T. F.: A large source of low-volatility secondary organic aerosol, Nature, 506,
1008 476-479, 10.1038/nature13032, 2014.

1009 Fetterer, F., K. Knowles, W. N. Meier, M. Savoie, and A. K. Windnagel. 2017, updated daily. *Sea Ice Index,*
1010 *Version 3*. [ftp://sidads.colorado.edu/DATASETS/NOAA/G02135/south/monthly/]. Boulder, Colorado USA.
1011 NSIDC: National Snow and Ice Data Center, 10.7265/N5K072F8, 2021 [last access: August 5, 2021].
1012

Fiebig, M., Hirdman, D., Lunder, C. R., Ogren, J. A., Solberg, S., Stohl, A., and Thompson, R. L.: Annual cycle of Antarctic baseline aerosol: controlled by photooxidation-limited aerosol formation, Atmos. Chem. Phys., 14, 3083-3093, 10.5194/acp-14-3083-2014, 2014.

Fiedler, V., Dal Maso, M., Boy, M., Aufmhoff, H., Hoffmann, J., Schuck, T., Birmili, W., Hanke, M., Uecker, J., Arnold, F., and Kulmala, M.: The contribution of sulphuric acid to atmospheric particle formation and growth: a comparison between boundary layers in Northern and Central Europe, Atmos. Chem. Phys., 5, 1773-1785, 10.5194/acp-5-1773-2005, 2005.

He, X.-C., Tham, Y. J., Dada, L., Wang, M., Finkenzeller, H., Stolzenburg, D., Iyer, S., Simon, M., Kürten, A., Shen, J., Rörup, B., Rissanen, M., Schobesberger, S., Baalbaki, R., Wang, D. S., Koenig, T. K., Jokinen, T., Sarnela, N., Beck, L. J., Almeida, J., Amanatidis, S., Amorim, A., Ataei, F., Baccarini, A., Bertozzi, B., Bianchi, F., Brilke, S., Caudillo, L., Chen, D., Chiu, R., Chu, B., Dias, A., Ding, A., Dommen, J., Duplissy, J., El Haddad, I., Gonzalez Carracedo, L., Granzin, M., Hansel, A., Heinritzi, M., Hofbauer, V., Junninen, H., Kangasluoma, J., Kemppainen, D., Kim, C., Kong, W., Krechmer, J. E., Kvashin, A., Laitinen, T., Lamkaddam, H., Lee, C. P., Lehtipalo, K., Leiminger, M., Li, Z., Makhmutov, V., Manninen, H. E., Marie, G., Marten, R., Mathot, S., Mauldin, R. L., Mentler, B., Möhler, O., Müller, T., Nie, W., Onnela, A., Petäjä, T., Pfeifer, J., Philippov, M., Ranjithkumar, A., Saiz-Lopez, A., Salma, I., Scholz, W., Schuchmann, S., Schulze, B., Steiner, G., Stozhkov, Y., Tauber, C., Tomé, A., Thakur, R. C., Väisänen, O., Vazquez-Pufleau, M., Wagner, A. C., Wang, Y., Weber, S. K., Winkler, P. M., Wu, Y., Xiao, M., Yan, C., Ye, Q., Ylisirniö, A., Zauner-Wieczorek, M., Zha, Q., Zhou, P., Flagan, R. C., Curtius, J., Baltensperger, U., Kulmala, M., Kerminen, V.-M., Kurtén, T., Donahue, N. M., Volkamer, R., Kirkby, J., Worsnop, D. R., and Sipilä, M.: Role of iodine oxoacids in atmospheric aerosol nucleation, Science, 371, 589, 10.1126/science.abe0298, 2021.

Herenz, P., Wex, H., Mangold, A., Laffineur, Q., Gorodetskaya, I. V., Fleming, Z. L., Panagi, M., and Stratmann, F.: CCN measurements at the Princess Elisabeth Antarctica research station during three austral summers, Atmos. Chem. Phys., 19, 275-294, 10.5194/acp-19-275-2019, 2019.

Hodshire, A. L., Campuzano-Jost, P., Kodros, J. K., Croft, B., Nault, B. A., Schroder, J. C., Jimenez, J. L., and Pierce, J. R.: The potential role of methanesulfonic acid (MSA) in aerosol formation and growth and the associated radiative forcings, Atmos. Chem. Phys., 19, 3137-3160, 10.5194/acp-19-3137-2019, 2019.

IPCC, Stocker, T. F., Qin, D., Plattner, G.-K., Tignor, M., Allen, S. K., Boschung, J., Nauels, A., Xia, Y., Bex, V., and Midgley, P. M. (Eds.): Climate Change 2013: The Physical Science Basis. Contribution of Working Group I to the Fifth Assessment Report of the Intergovernmental Panel on Climate Change, Cambridge University Press, Cambridge, United Kingdom and New York, NY, USA, 1535 pp., 10.1017/CBO9781107415324, 2013.

Jokinen, T., Sipilä, M., Junninen, H., Ehn, M., Lönn, G., Hakala, J., Petäjä, T., Mauldin Iii, R. L., Kulmala, M., and Worsnop, D. R.: Atmospheric sulphuric acid and neutral cluster measurements using CI-APi-TOF, Atmos. Chem. Phys., 12, 4117-4125, 10.5194/acp-12-4117-2012, 2012.

Jokinen, T., Sipilä, M., Kontkanen, J., Vakkari, V., Tisler, P., Duplissy, E. M., Junninen, H., Kangasluoma, J., Manninen, H. E., Petäjä, T., Kulmala, M., Worsnop, D. R., Kirkby, J., Virkkula, A., and Kerminen, V. M.: Ion-induced sulfuric acid–ammonia nucleation drives particle formation in coastal Antarctica, Science Advances, 4, eaat9744, 10.1126/sciadv.aat9744, 2018.

Järvinen, E., Virkkula, A., Nieminen, T., Aalto, P. P., Asmi, E., Lanconelli, C., Busetto, M., Lupi, A., Schioppo, R., Vitale, V., Mazzola, M., Petäjä, T., Kerminen, V. M., and Kulmala, M.: Seasonal cycle and modal structure of particle number size distribution at Dome C, Antarctica, Atmos. Chem. Phys., 13, 7473-7487, 10.5194/acp-13-7473-2013, 2013.

Kangasluoma, J., Franchin, A., Duplissy, J., Ahonen, L., Korhonen, F., Attoui, M., Mikkilä, J., Lehtipalo, K., Vanhanen, J., Kulmala, M., and Petäjä, T.: Operation of the Airmodus A11 nano Condensation Nucleus Counter at various inlet pressures and various operation temperatures, and design of a new inlet system, Atmos. Meas. Tech., 9, 2977-2988, 10.5194/amt-9-2977-2016, 2016.

Kecorius, S., Vogl, T., Paasonen, P., Lampilahti, J., Rothenberg, D., Wex, H., Zeppenfeld, S., van Pinxteren, M., Hartmann, M., Henning, S., Gong, X., Welti, A., Kulmala, M., Stratmann, F., Herrmann, H., and Wiedensohler, A.: New particle formation and its effect on cloud condensation nuclei abundance in the summer Arctic: a case study in the Fram Strait and Barents Sea, Atmos. Chem. Phys., 19, 14339-14364, 10.5194/acp-19-14339-2019, 2019.

Kerminen, V.-M., Chen, X., Vakkari, V., Petäjä, T., Kulmala, M., and Bianchi, F.: Atmospheric new particle formation and growth: review of field observations, Environmental Research Letters, 13, 103003, 10.1088/1748-9326/aadf3c, 2018.

Kirkby, J., Curtius, J., Almeida, J., Dunne, E., Duplissy, J., Ehrhart, S., Franchin, A., Gagné, S., Ickes, L., Kürten, A., Kupc, A., Metzger, A., Riccobono, F., Rondo, L., Schobesberger, S., Tsagkogeorgas, G., Wimmer, D., Amorim, A., Bianchi, F., Breitenlechner, M., David, A., Dommen, J., Downard, A., Ehn, M., Flagan, R. C., Haider, S., Hansel, A., Hauser, D., Jud, W., Junninen, H., Kreissl, F., Kvashin, A., Laaksonen, A., Lehtipalo, K., Lima, J., Lovejoy, E. R., Makhmutov, V., Mathot, S., Mikkilä, J., Minginette, P., Mogo, S., Nieminen, T., Onnela, A., Pereira, P., Petäjä, T., Schnitzhofer, R., Seinfeld, J. H., Sipilä, M., Stozhkov, Y., Stratmann, F., Tomé, A., Vanhanen, J., Viisanen, Y., Vrtala, A., Wagner, P. E., Walther, H., Weingartner, E., Wex, H., Winkler, P. M., Carslaw, K. S., Worsnop, D. R., Baltensperger, U., and Kulmala, M.: Role of sulphuric acid, ammonia and galactic cosmic rays in atmospheric aerosol nucleation, Nature, 476, 429-433, 10.1038/nature10343, 2011.

Kirkby, J., Duplissy, J., Sengupta, K., Frege, C., Gordon, H., Williamson, C., Heinritzi, M., Simon, M., Yan, C., Almeida, J., Tröstl, J., Nieminen, T., Ortega, I. K., Wagner, R., Adamov, A., Amorim, A., Bernhammer, A.-K., Bianchi, F., Breitenlechner, M., Brilke, S., Chen, X., Craven, J., Dias, A., Ehrhart, S., Flagan, R. C., Franchin, A., Fuchs, C., Guida, R., Hakala, J., Hoyle, C. R., Jokinen, T., Junninen, H., Kangasluoma, J., Kim, J., Krapf, M., Kürten, A., Laaksonen, A., Lehtipalo, K., Makhmutov, V., Mathot, S., Molteni, U., Onnela, A., Peräkylä, O., Piel, F., Petäjä, T., Praplan, A. P., Pringle, K., Rap, A., Richards, N. A. D., Riipinen, I., Rissanen, M. P., Rondo, L., Sarnela, N., Schobesberger, S., Scott, C. E., Seinfeld, J. H., Sipilä, M., Steiner, G., Stozhkov, Y., Stratmann, F., Tomé, A., Virtanen, A., Vogel, A. L., Wagner, A. C., Wagner, P. E., Weingartner, E., Wimmer, D., Winkler, P. M., Ye, P., Zhang, X., Hansel, A., Dommen, J., Donahue, N. M., Worsnop, D. R., Baltensperger, U., Kulmala, M., Carslaw, K. S., and Curtius, J.: Ion-induced nucleation of pure biogenic particles, Nature, 533, 521-526, 10.1038/nature17953, 2016.

Kontkanen, J., Järvinen, E., Manninen, H. E., Lehtipalo, K., Kangasluoma, J., Decesari, S., Gobbi, G. P., Laaksonen, A., Petäjä, T., and Kulmala, M.: High concentrations of sub-3nm clusters and frequent new particle formation observed in the Po Valley, Italy, during the PEGASOS 2012 campaign, Atmos. Chem. Phys., 16, 1919-1935, 10.5194/acp-16-1919-2016, 2016.

Kulmala, M., Kontkanen, J., Junninen, H., Lehtipalo, K., Manninen, H. E., Nieminen, T., Petäjä, T., Sipilä, M., Schobesberger, S., and Rantala, P.: Direct observations of atmospheric aerosol nucleation, Science, 339, 943-946, 10.1126/science.1227385, 2013.

Kulmala, M., Petäjä, T., Nieminen, T., Sipilä, M., Manninen, H. E., Lehtipalo, K., Dal Maso, M., Aalto, P. P., Junninen, H., Paasonen, P., Riipinen, I., Lehtinen, K. E. J., Laaksonen, A., and Kerminen, V.-M.: Measurement of the nucleation of atmospheric aerosol particles, Nature Protocols, 7, 1651-1667, 10.1038/nprot.2012.091, 2012.

Kulmala, M., Stolzenburg, D., Dada, L., Cai, R., Kontkanen, J., Yan, C., Kangasluoma, J., Ahonen, L. R., Gonzalez-Carracedo, L., Sulo, J., Tuovinen, S., Deng, C., Li, Y., Lehtipalo, K., Lehtinen, K. E. J., Petäjä, T., Winkler, P. M., Jiang, J., and Kerminen, V.-M.: Towards a concentration closure of sub-6 nm aerosol particles and sub-3 nm atmospheric clusters, Journal of Aerosol Science, 159, 105878, 10.1016/j.jaerosci.2021.105878, 2022.

Kyrö, E. M., Kerminen, V. M., Virkkula, A., Dal Maso, M., Parshintsev, J., Ruíz-Jimenez, J., Forsström, L., Manninen, H. E., Riekkola, M. L., Heinonen, P., and Kulmala, M.: Antarctic new particle formation from continental biogenic precursors, Atmos. Chem. Phys., 13, 3527-3546, 10.5194/acp-13-3527-2013, 2013.

Kürten, A.: New particle formation from sulfuric acid and ammonia: nucleation and growth model based on thermodynamics derived from CLOUD measurements for a wide range of conditions, Atmos. Chem. Phys., 19, 5033-5050, 10.5194/acp-19-5033-2019, 2019.

Kürten, A., Jokinen, T., Simon, M., Sipilä, M., Sarnela, N., Junninen, H., Adamov, A., Almeida, J., Amorim, A., Bianchi, F., Breitenlechner, M., Dommen, J., Donahue, N. M., Duplissy, J., Ehrhart, S., Flagan, R. C., Franchin, A., Hakala, J., Hansel, A., Heinritzi, M., Hutterli, M., Kangasluoma, J., Kirkby, J., Laaksonen, A., Lehtipalo, K., Leiminger, M., Makhmutov, V., Mathot, S., Onnela, A., Petäjä, T., Praplan, A. P., Riccobono, F., Rissanen, M. P., Rondo, L., Schobesberger, S., Seinfeld, J. H., Steiner, G., Tomé, A., Tröstl, J., Winkler, P. M., Williamson, C., Wimmer, D., Ye, P., Baltensperger, U., Carslaw, K. S., Kulmala, M., Worsnop, D. R., and Curtius, J.: Neutral molecular cluster formation of sulfuric acid–dimethylamine observed in real time under atmospheric conditions, Proceedings of the National Academy of Sciences, 111, 15019, 10.1073/pnas.1404853111, 2014.

Lachlan-Cope, T., Beddows, D. C. S., Brough, N., Jones, A. E., Harrison, R. M., Lupi, A., Yoon, Y. J., Virkkula, A., and Dall'Osto, M.: On the annual variability of Antarctic aerosol size distributions at Halley Research Station, Atmos. Chem. Phys., 20, 4461-4476, 10.5194/acp-20-4461-2020, 2020.

Lana, A., Bell, T. G., Simó, R., Vallina, S. M., Ballabrera-Poy, J., Kettle, A. J., Dachs, J., Bopp, L., Saltzman, E. S., Stefels, J., Johnson, J. E., and Liss, P. S.: An updated climatology of surface dimethlysulfide concentrations and emission fluxes in the global ocean, Global Biogeochemical Cycles, 25, 10.1029/2010GB003850, 2011.

Lehtipalo, K., Leppa, J., Kontkanen, J., Kangasluoma, J., Franchin, A., Wimnner, D., Schobesberger, S., Junninen, H., Petaja, T., and Sipila, M.: Methods for determining particle size distribution and growth rates between 1 and 3 nm using the Particle Size Magnifier, Boreal Environment Research, 2014.

Lehtipalo, K., Ahonen, L. R., Baalbaki, R., Sulo, J., Chan, T., Laurila, T., Dada, L., Duplissy, J., Miettinen, E., Vanhanen, J., Kangasluoma, J., Kulmala, M., Petäjä, T., and Jokinen, T.: The standard operating procedure for Airmodus Particle Size Magnifier and nano-Condensation Nucleus Counter, Journal of Aerosol Science, 159, 105896, 10.1016/j.jaerosci.2021.105896, 2022.

Loo, B. W. and Cork, C. P.: Development of High Efficiency Virtual Impactors, Aerosol Science and Technology, 9, 167-176, 10.1080/02786828808959205, 1988.

Manninen, H. E., Mirme, S., Mirme, A., Petäjä, T., and Kulmala, M.: How to reliably detect molecular clusters and nucleation mode particles with Neutral cluster and Air Ion Spectrometer (NAIS), Atmos. Meas. Tech., 9, 3577-3605, 10.5194/amt-9-3577-2016, 2016.

Mardyukov, A. and Schreiner, P. R.: Atmospherically Relevant Radicals Derived from the Oxidation of Dimethyl Sulfide, Accounts of Chemical Research, 51, 475-483, 10.1021/acs.accounts.7b00536, 2018.

Merikanto, J., Spracklen, D. V., Mann, G. W., Pickering, S. J., and Carslaw, K. S.: Impact of nucleation on global CCN, Atmos. Chem. Phys., 9, 8601-8616, 10.5194/acp-9-8601-2009, 2009.

Mirme, S. and Mirme, A.: The mathematical principles and design of the NAIS – a spectrometer for the measurement of cluster ion and nanometer aerosol size distributions, Atmos. Meas. Tech., 6, 1061-1071, 10.5194/amt-6-1061-2013, 2013.

Notz, D.: The future of ice sheets and sea ice: Between reversible retreat and unstoppable loss, Proceedings of the National Academy of Sciences, 106, 20590-20595, 10.1073/pnas.0902356106, 2009.

Saiz-Lopez, A. and von Glasow, R.: Reactive halogen chemistry in the troposphere, Chemical Society Reviews, 41, 6448-6472, 10.1039/C2CS35208G, 2012.

Saiz-Lopez, A., Blaszczak-Boxe, C. S., and Carpenter, L. J.: A mechanism for biologically induced iodine emissions from sea ice, Atmos. Chem. Phys., 15, 9731-9746, 10.5194/acp-15-9731-2015, 2015.

Saiz-Lopez, A., Mahajan Anoop, S., Salmon Rhian, A., Bauguitte Stephane, J. B., Jones Anna, E., Roscoe Howard, K., and Plane John, M. C.: Boundary Layer Halogens in Coastal Antarctica, Science, 317, 348-351, 10.1126/science.1141408, 2007.

Schmale, J., Baccarini, A., Thurnherr, I., Henning, S., Efraim, A., Regayre, L., Bolas, C., Hartmann, M., Welti, A., Lehtipalo, K., Aemisegger, F., Tatzelt, C., Landwehr, S., Modini, R. L., Tummon, F., Johnson, J. S., Harris, N., Schnaiter, M., Toffoli, A., Derkani, M., Bukowiecki, N., Stratmann, F., Dommen, J., Baltensperger, U., Wernli, H., Rosenfeld, D., Gysel-Beer, M., and Carslaw, K. S.: Overview of the Antarctic Circumnavigation Expedition: Study of Preindustrial-like Aerosols and Their Climate Effects (ACE-SPACE), Bulletin of the American Meteorological Society, 100(11), 2260-2283, 10.1175/BAMS-D-18-0187.1, 2019.

Schobesberger, S., Junninen, H., Bianchi, F., Lönn, G., Ehn, M., Lehtipalo, K., Dommen, J., Ehrhart, S., Ortega, I., Franchin, A., Nieminen, T., Riccobono, F., Hutterli, M., Duplissy, J., Almeida, J., Amorim, A., Breitenlechner, M., Downard, A., Dunne, E., and Worsnop, D.: Molecular understanding of atmospheric particle formation from sulfuric acid and large oxidized organic molecules, Proceedings of the National Academy of Sciences of the United States of America, 10.1073/pnas.1306973110, 2013.

Schobesberger, S., Franchin, A., Bianchi, F., Rondo, L., Duplissy, J., Kürten, A., Ortega, I. K., Metzger, A., Schnitzhofer, R., Almeida, J., Amorim, A., Dommen, J., Dunne, E. M., Ehn, M., Gagné, S., Ickes, L., Junninen, H., Hansel, A., Kerminen, V. M., Kirkby, J., Kupc, A., Laaksonen, A., Lehtipalo, K., Mathot, S., Onnela, A., Petäjä, T., Riccobono, F., Santos, F. D., Sipilä, M., Tomé, A., Tsagkogeorgas, G., Viisanen, Y., Wagner, P. E., Wimmer, D., Curtius, J., Donahue, N. M., Baltensperger, U., Kulmala, M., and Worsnop, D. R.: On the composition of ammonia–sulfuric-acid ion clusters during aerosol particle formation, Atmos. Chem. Phys., 15, 55-78, 10.5194/acp-15-55-2015, 2015.

Shaw, G. E.: Considerations on the origin and properties of the Antarctic aerosol, Reviews of Geophysics, 17, 1983-1998, 10.1029/RG017i008p01983, 1979.

Shaw, G. E.: Antarctic aerosols: A review, Reviews of Geophysics, 26, 89-112, 10.1029/RG026i001p00089, 1988.

Sipilä, M., Berndt, T., Petäjä, T., Brus, D., Vanhanen, J., Stratmann, F., Patokoski, J., Mauldin, R. L., Hyvärinen, A.-P., Lihavainen, H., and Kulmala, M.: The Role of Sulfuric Acid in Atmospheric Nucleation, Science, 327, 1243, 10.1126/science.1180315, 2010.

Sipilä, M., Sarnela, N., Neitola, K., Laitinen, T., Kemppainen, D., Beck, L., Duplissy, E. M., Kuittinen, S., Lehmusjärvi, T., Lampilahti, J., Kerminen, V. M., Lehtipalo, K., Aalto, P. P., Keronen, P., Siivola, E., Rantala, P. A., Worsnop, D. R., Kulmala, M., Jokinen, T., and Petäjä, T.: Wintertime sub-arctic new particle formation from Kola Peninsula sulphur emissions, Atmos. Chem. Phys. Discuss., 2021, 1-27, 10.5194/acp-2020-1202, 2021.

Sipilä, M., Sarnela, N., Jokinen, T., Henschel, H., Junninen, H., Kontkanen, J., Richters, S., Kangasluoma, J., Franchin, A., Peräkylä, O., Rissanen, M. P., Ehn, M., Vehkamäki, H., Kurten, T., Berndt, T., Petäjä, T., Worsnop, D., Ceburnis, D., Kerminen, V.-M., Kulmala, M., and O'Dowd, C.: Molecular-scale evidence of aerosol particle formation via sequential addition of HIO3, Nature, 537, 532-534, 10.1038/nature19314, 2016.

Stuecker, M. F., Bitz, C. M., Armour, K. C., Proistosescu, C., Kang, S. M., Xie, S.-P., Kim, D., McGregor, S., Zhang, W., Zhao, S., Cai, W., Dong, Y., and Jin, F.-F.: Polar amplification dominated by local forcing and feedbacks, Nature Climate Change, 8, 1076-1081, 10.1038/s41558-018-0339-y, 2018.

Vanhanen, J., Mikkilä, J., Lehtipalo, K., Sipilä, M., Manninen, H. E., Siivola, E., Petäjä, T., and Kulmala, M.: Particle Size Magnifier for Nano-CN Detection, Aerosol Science and Technology, 45, 533-542, 10.1080/02786826.2010.547889, 2011.

Virkkula, A., Asmi, E., Teinilä, K., Frey, A., Aurela, M., Timonen, H., Mäkelä, T., Samuli, A., Hillamo, R., Aalto, P., Kirkwood, S., and Kulmala, M.: Review of Aerosol Research at the Finnish Antarctic Research Station Aboa and its Surroundings in Queen Maud Land, Antarctica, Geophysica, 45, 2009.

Von Berg, L., Prend, C. J., Campbell, E. C., Mazloff, M. R., Talley, L. D., and Gille, S. T.: Weddell Sea Phytoplankton Blooms Modulated by Sea Ice Variability and Polynya Formation, Geophysical Research Letters, 47, e2020GL087954, 10.1029/2020GL087954, 2020.

Weller, R., Schmidt, K., Teinilä, K., and Hillamo, R.: Natural new particle formation at the coastal Antarctic site Neumayer, Atmos. Chem. Phys., 15, 11399-11410, 10.5194/acp-15-11399-2015, 2015.

Wiedensohler, A., Birmili, W., Nowak, A., Sonntag, A., Weinhold, K., Merkel, M., Wehner, B., Tuch, T., Pfeifer, S., Fiebig, M., Fjäraa, A. M., Asmi, E., Sellegri, K., Depuy, R., Venzac, H., Villani, P., Laj, P., Aalto, P., Ogren, J. A., Swietlicki, E., Williams, P., Roldin, P., Quincey, P., Hüglin, C., Fierz-Schmidhauser, R., Gysel, M., Weingartner, E., Riccobono, F., Santos, S., Grüning, C., Faloon, K., Beddows, D., Harrison, R., Monahan, C., Jennings, S. G., O'Dowd, C. D., Marinoni, A., Horn, H. G., Keck, L., Jiang, J., Scheckman, J., McMurry, P. H., Deng, Z., Zhao, C. S., Moerman, M., Henzing, B., de Leeuw, G., Löschau, G., and Bastian, S.: Mobility particle size spectrometers: harmonization of technical standards and data structure to facilitate high quality long-term observations of atmospheric particle number size distributions, Atmos. Meas. Tech., 5, 657-685, 10.5194/amt-5-657-2012, 2012.

Willis, M. D., Burkart, J., Thomas, J. L., Köllner, F., Schneider, J., Bozem, H., Hoor, P. M., Aliabadi, A. A., Schulz, H., Herber, A. B., Leaitch, W. R., and Abbatt, J. P. D.: Growth of nucleation mode particles in the summertime Arctic: a case study, Atmos. Chem. Phys., 16, 7663-7679, 10.5194/acp-16-7663-2016, 2016.

Yan, C., Dada, L., Rose, C., Jokinen, T., Nie, W., Schobesberger, S., Junninen, H., Lehtipalo, K., Sarnela, N., Makkonen, U., Garmash, O., Wang, Y., Zha, Q., Paasonen, P., Bianchi, F., Sipilä, M., Ehn, M., Petäjä, T., Kerminen, V. M., Worsnop, D. R., and Kulmala, M.: The role of H2SO4-NH3 anion clusters in ion-induced aerosol nucleation mechanisms in the boreal forest, Atmos. Chem. Phys., 18, 13231-13243, 10.5194/acp-18-13231-2018, 2018.

Yu, H., Ortega, J., Smith, J. N., Guenther, A. B., Kanawade, V. P., You, Y., Liu, Y., Hosman, K., Karl, T., Seco, R., Geron, C., Pallardy, S. G., Gu, L., Mikkilä, J., and Lee, S.-H.: New Particle Formation and Growth in an Isoprene-Dominated Ozark Forest: From Sub-5 nm to CCN-Active Sizes, Aerosol Science and Technology, 48, 1285-1298, 10.1080/02786826.2014.984801, 2014.